Sample-holder design and proof-of-principle experiments with protons: biology versus dosimetry

Nicky van Lobenstein

TU Delft
Erasmus MC
Universitair Medisch Centrum Rotterdam

Sample-holder design and proof-of-principle experiments with protons: biology versus dosimetry

by

Nicky van Lobenstein

in partial fulfillment of the requirements for the degree of

Master of Science
in Biomedical Engineering
Medical Physics

at the Delft University of Technology,
to be defended publicly on Wednesday July 17th, 2019 at 13:00h.

Student number:	4432827
Project duration:	November 19th, 2018 - July 17th, 2019
Performed at:	Erasmus MC Rotterdam, Radiotherapy department

Thesis committee

Chairman:	Prof. dr. H.Th. Wolterbeek	TU Delft, Applied Sciences, ARI
1st supervisor:	dr. D. Lathouwers	TU Delft, Applied Sciences, RPNM
2nd supervisor:	dr. Z. Perko	TU Delft, Applied Sciences, RPNM
3rd supervisor:	dr. S. Habraken	Erasmus MC, Rad. Oncol. Physics
4th supervisor:	dr. D.C. van Gent	Erasmus MC, Molecular Genetics

TU Delft

Erasmus MC
Universitair Medisch Centrum Rotterdam

Abstract

Purpose/objective The aim of the thesis project is to design and build a sample-holder that is suited for radiobiological experiments on cell and tissue level in Holland PTC. In order to create accurate dose plans for radiobiological experiments, dosimetry and range calculations need to be worked out. Finally the sample-holder is used for the first radiobiological experiment at Holland PTC.

Material and Methods The sample-holder is constructed as a slab phantom that allows secure and easy positioning of a 6-well cultivating plate, fully made out of polystyrene. Water equivalent thickness (WET) measurements are used to calculate the density of the slabs, which can be used for dose calculations in treatment planning and Monte Carlo software. Radiochromic EBT3 film is used to perform dosimetry during experiments, the films are calibrated using an ionization chamber to be able to perform absolute dosimetry. A 70 MeV single pencil beam is delivered to the sample-holder with EBT3 films in between the slabs to compare a reconstructed Bragg peak from the relative doses of the films with dose calculations performed in RayStation and TOPAS MC. Cell survival experiments with U2OS cells are performed by irradiating with X-rays and protons. Circumstances where such that the influence of cells being on room temperature for several hours and cells being without medium inside the wells during irradiation could be studied. With protons, cells were irradiated both in the plateau region and in the Bragg peak. LET_d calculations are performed in TOPAS MC in order to study the RBE-LET relation.

Results The slabs of the phantom are uniform and have a density of either 1.04 g/cm^3 or 1.06 g/cm^3. Using these density values the range of a 70 MeV can be calculated with a 0.5 mm accuracy using TOPAS MC and RayStation. The relative central axis dose profile calculated with TOPAS was accurate within 5% compared to the measured values with EBT3 film. This was 20% for calculations with RayStation. Absolute dose measurements with EBT3 film inside a RW3 phantom agree within 1% with the delivered dose according to the ionization chamber. In the polystyrene sample-holder this difference is 11%. For X-ray irradiation, incubated cells were able to form more colonies after irradiation compared to cells that had been on room temperature for four hours. Cells that were irradiated without medium in the well had a higher surviving fraction than cells that had medium in the well. For proton irradiation the results are limited since all cells that received more than 0.91 Gy had died, but from the available data it can be seen that irradiation in the Bragg peak results in more cell death compared to irradiation in the plateau region. In addition to this, cells that had medium in the wells during irradiation formed less colonies than cells that had no medium in the wells, which is consistent with the results after X-ray irradiation. Dose-averaged LET (LET_d) values are calculated at cell depth for proton irradiation in the plateau region and in the Bragg peak and are 1.30 keV/μm and 3.78 keV/μm respectively.

Conclusion The sample-holder is well defined for use in RayStation and TOPAS MC and range calculations of a 70 MeV pencil beam are accurate within 0.5 mm. Absolute dose values obtained with EBT3 film inside the sample-holder are higher than expected, additional measurements are recommended. Cell survival experiments show that there is a difference in irradiating cells that are in medium vs cells that are not in medium and that long exposure to room temperature increases cell death after irradiation. Radiobiological experiments should be performed with cells that can be prepared and stored on site. The obtained LET_d values are comparable with values found in literature. Due to the limited amount of cell survival data after proton irradiation, not link between RBE and LET can be studied.

Contents

Introduction

Proton beam therapy is a type of external radiation therapy where protons are used to treat cancer rather than X-ray beams or γ-sources. The main advantage of protons over photons is that the radiation dose can be delivered to the tumor with better conformality. This means that with protons, a tumor can be targeted while sparing more healthy tissue compared to irradiation with photons. Details on this difference in dose deposition and the underlying physics are treated in Section 1.1. The potential of protons (and other charged particles) to be an effective tool in fighting cancer was already described in 1946 by Robert R. Wilson [1], but has only been introduced as a treatment method in the Netherlands in 2018. This large gap between discovery and clinical application can be attributed to three main challenges of proton therapy: (a) The high financial cost of the treatment modality, (b) the range uncertainty caused by imaging, patient setup, beam delivery and dose calculation [2] and (c) the understudied biological effect induced by proton radiation [3]. The focus of this thesis project will be the understudied biological effect of protons.

Worldwide the access to proton therapy centers for biological *in vitro* experiments is limited. This is, among others, due to the fact that most centers are treatment facilities and need a financial return for the expensive treatment modality [4]. Despite being a treatment facility in the first place, Holland PTC in Delft is built with the strong requirement to perform research to prove the benefit of proton therapy [5]. The aim of this thesis project is to design and build a sample-holder and contribute to the first radiobiological experiments at Holland PTC. Thanks to its consortium that consists of two University Medical Centers (Erasmus MC & Leiden UMC) and the Technical University of Delft, Holland PTC has the means to perform this research and contribute to the necessary experiments for a better understanding of proton radiobiology.

A brief introduction on the energy loss of protons, proton radiobiology, Monte Carlo simulations and dosimetry is given in Chapter 1. Because radiobiological experiments have never before been conducted in Holland PTC, extra care is needed in setting up these experiments. A literature study is conducted on how to conduct radiobiological experiments in proton therapy and how to design the experiments in such a way that the results will be relevant to the clinical situation. This literature study is included as Chapter 2 in this thesis. Questions that are addressed in this literature study are:

1. How do other centers conduct radiobiological experiments on cellular level?
2. How can results from fundamental experiments be translated to the clinic?

In Chapter 3 and Chapter 4 is elaborated on the materials & methods and results respectively. This includes the considerations and choices that were made for the sample-holder design, the dosimetric validation and modelling of the sample-holder, the models and physics used for Monte Carlo LET calculations and finally the experimental plan for the radiobiolical experiments at Holland PTC.

1 Proton energy loss, radiobiology and dosimetry

The physical behaviour of protons in the human body, and therefore the biological effect it induces, is different compared to photons. Both physically and biologically, the behaviour of protons is different compared to photons. The aim of this chapter is to provide the reader with the necessary background knowledge of the physical behaviour of protons and its biological effect.

1.1 Energy loss of protons

Because of a proton's mass and charge it loses energy through different interactions with the traversing medium than photons, which result in different depth dose distributions. The depth dose deposition of 15 MV X-rays and a 200 MeV proton pristine- and spread-out Bragg peak are visualized in Figure 2. Contrary to X-rays, the energy deposition of particles increases with depth. This phenomenon was first described for alpha particles by Bragg in 1903[6], which is why the peak at the end of the proton range is called the 'Bragg peak'. This different depth dose distribution allows for more conformal dose delivery to a region of interest, which was the initial argument for using particle beams for medical treatment by Robert R. Wilson in 1946[1]. Looking at Figure 18, it is evident that the dose deposition of protons allows for better sparing of healthy tissue in front and behind the tumor than X-rays.

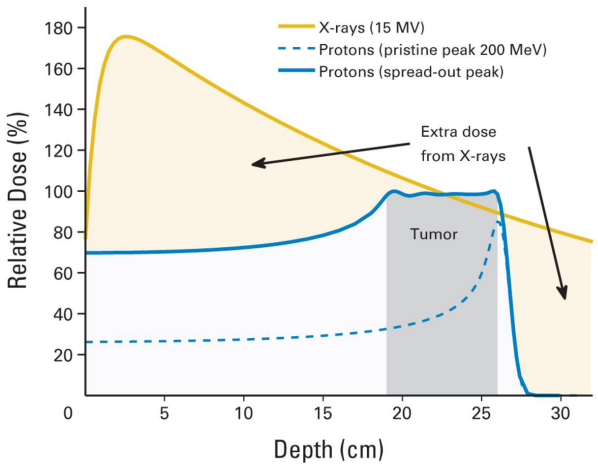

Figure 2: Depth dose distributions of photons and protons[7].

The absorbed dose of ionizing radiation to matter is the deposited energy per unit mass, as shown in Formula 1.

$$D = \frac{E}{m}, \tag{1}$$

where D is the dose in Gray (Gy), E is the energy in Joule and m is the mass in kilograms. The energy loss of a charged particle for therapeutically relevant energies

can be described by the Bethe-Bloch formula[8–10]:

$$-\frac{dE}{dx} = \frac{4\pi e^4 Z_{eff}^2 Z_t N}{m_e v^2}\left[\ln\left(\frac{2mc^2\beta^2}{I(1-\beta)}\right) - \beta^2\right], \tag{2}$$

where $\frac{dE}{dx}$ is the energy loss per unit distance traveled, Z_t is the effective atomic number of the target, N the electron density of the target, m_e and e are the mass and charge of the electron, v is the projectile velocity, $\beta = \frac{v}{c}$ and I is the mean excitation potential. The effective atomic number of the projectile Z_{eff} changes at low velocities (order of the Bohr velocity), when the protons start binding with electrons from the target, reducing its charge and thus also reducing the stopping power. Z_{eff} can be approximated by the Barkas formula[11]:

$$Z_{eff} = Z(1 - e^{-125\beta Z^{-\frac{2}{3}}}) \tag{3}$$

The energy loss per unit length calculated in Formula (2) is called the stopping power:

$$S(E) = -\frac{dE}{dx}. \tag{4}$$

Both the electronic and nuclear stopping power are shown in Figure 3 as a function of proton kinetic energy. Electronic stopping refers to the slowing down of a projectile ion due to the inelastic collisions with bound electrons in the medium. Nuclear stopping, which contributes very little to the total stopping, refers to the elastic collisions between the projectile ion and nuclei in the sample[12].

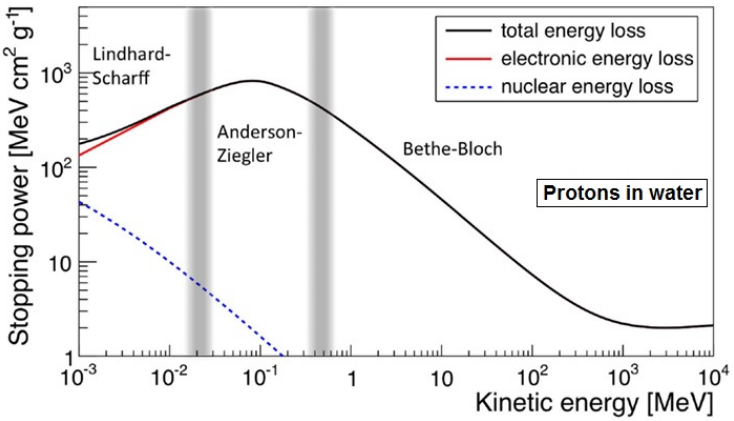

Figure 3: Stopping power (dE/dx) for protons in water as function of kinetic energy. The total, electronic, and nuclear stopping power are shown, as well as the characteristic regions. Figure from Kraan (2015)[12], made using NIST data[13].

1.1.1 Linear energy transfer

The stopping power is used to calculate an important parameter in proton radiobiology: the Linear energy transfer (LET), in keV/μm. The (restricted) LET$_\delta$ is defined as the energy lost by a particle in a material, due to secondary electrons with an

energy less than δ, over a certain distance[14]. If δ tends towards infinity, the LET becomes unrestricted and is identical to the linear electronic stopping power. It can be seen in Figure 3 that as the kinetic energy of the proton decreases, the stopping power and thus LET increases (for protons with energies higher than 0.1 MeV). This inverse proportionality causes the LET to strongly increase just before the end of the particle trajectory, as shown in Figure 4. LET_δ is well defined for ions with a fixed

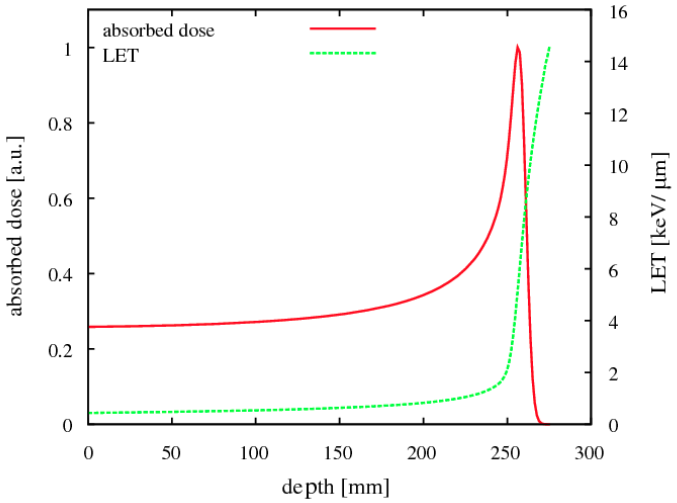

Figure 4: Depth dose curve and dose-averaged LET for a 200 MeV proton beam in water, from Frese *et al* (2011)[15].

energy, however in proton therapy we generally deal with a radiation field of mixed particles over a wide range of energies. In mixed radiation fields the contributions of the different energies to the LET have to be averaged[16]. Two averaged LET measures are generally applied: the track-averaged LET and dose-averaged LET referred to as LET_t and LET_d. When using the LET as a biological predictor, both dose and LET have to be considered. The LET_d is chosen as a biological predictor, as the LET_d takes into account both dose and LET where the LET_t does not take into account dose[17]. The LET_d per particle type is defined[18] as

$$LET_d(z) = \frac{\int_0^\infty S_{el}^2(E)\Phi(E,z)dE}{\int_0^\infty S_{el}(E)\Phi(E,z)dE}, \tag{5}$$

where $S_{el}(E)$ is the electronic stopping power of primary charged particles with kinetic energy E, $D(E,z)$ is the absorbed dose contributed by primary charged particles with kinetic energy E at position z and $\Phi(E,z)$ is the fluence of primary charged particles with kinetic energy E at position z. The LET_t per particle type is defined[18] as

$$LET_t(z) = \frac{\int_0^\infty S_{el}(E)\Phi(E,z)dE}{\int_0^\infty \Phi(E,z)dE}. \tag{6}$$

1.2 Proton radiobiology

Although the differences in biological response to proton and photon radiation have been studied in the past few years (see Chapter 2), the radiobiological aspects of

proton therapy need better understanding in order to fully utilize its potential. It is assumed that increased knowledge on the cell and tissue response to proton radiation can improve clinical results of proton beam therapy[19]. This section discusses DNA damage and repair as well as a cell survival model and a method quantify the biological effect of protons.

1.2.1 DNA damage and cell kill

Three main factors determine the biological effect of ionizing radiation inside the body: ionizations that are close enough to the DNA to directly damage it, free radical scavenging processes and cellular repair processes. When free-radicals created by the ionization of surrounding molecules damage the DNA, this is considered indirect damage[20]. Radiation can induce various types of DNA damage of which the most common ones are base damages, single-strand breaks (SSB) and double-strand breaks (DSB). As DSB are harder to repair than SSB, DSB are considered the most prominent cause biological effects due to ionizing radiation[21–23]. When multiple damage sites are densely spaced they can induce a clustered lesion. Clustered lesions are considered to be extra hard to repair and are mainly responsible for lethal and mutagenic effects[24–26]. Densely spaced ionizations are induced by high-LET radiation, as can be seen in Figure 5. For high-LET radiation such as neutrons or

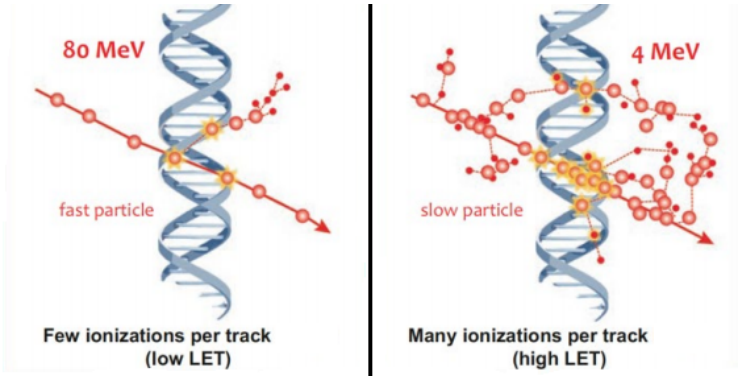

Figure 5: The difference in ionization density between low- and high-LET radiation, visualized as one particle that interacts with DNA strands. Figure from[27]

α-particles, direct DNA damage is dominant. For low-LET radiation such as X-rays or electrons, indirect DNA damage is dominant. Protons are considered low-LET in the plateau region, but as their energy decreases and they approach the end of their track, the LET increases and they are considered high-LET particles. DNA damage due to direct ionizations often lead to DSB, where damage due to free-radical scavenging often leads do SSB.

An important factor related to biological response is DNA Double strand break DSB repair. There are two dominant pathways for repairing DSBs induced by ionizing radiation: Homologous Recombination (HR) and Non-Homologous End-Joining (NHEJ). In NHEJ, the open ends of the DNA strands are ligated together. In this process the resected base pairs are lost, resulting in incomplete repair. In homologous recombination, nucleotide sequences are exchanged between two DNA strands that contain

similar or identical base sequences. First up to 100 base pairs of the damaged sites are deleted, followed by a recombination protein that binds to a corresponding part of homologous DNA. Subsequently the missing base pairs are copied and the strands are recombined. Deficiency in a repair pathway results in an increased chance of cell mutation or necrosis. By combining a drug that inhibits one of these pathways, the biological effect of ionizing radiation can be increased.

1.2.2 Cell survival and RBE

The biological effect on a cellular level is generally described by the surviving fraction of cells after irradiation. The cell surviving fraction is often obtained by means of clonogenic assays. A clonogenic assay is the observation of a colony that derives from a single irradiated cell. At a cell dependent moment after the irradiation, the colonies are fixated and counted. The number of colonies is then compared to the number of cells that were seeded and the ratio between these numbers is the surviving fraction. Quantification of expected biological effect for a certain physical dose is important for treatment planning. For fraction doses up to a few Gray cell survival can be accurately described by the linear quadratic expression, where SF is the Surviving Fraction of cells for a certain dose D.

$$SF(D) = exp\{-\alpha D - \beta D^2\}, \tag{7}$$

with absorbed dose D and fitted coefficients α and β. The shoulder of the survival curve in Figure 6 describes the Relative Biological Effectiveness (RBE) of a particle with respect to photons. This curve depends on the ratio between α and β[28]. The values α and β vary per cell type, biological endpoint and type of radiation. The RBE is a measure to compare two treatment modalities, defined as the ratio of required doses to achieve the same biological effect. An example for RBE that is shown in Figure 6 is the RBE_{10}, which is the ratio between doses that are needed to achieve a surviving fraction of 10%. The coefficient α is proportional to the LET of the particle[29], the Wedenberg *et al* model[30] model for instance assumes a linear relationship between α and the LET. This means that LET and RBE are related.

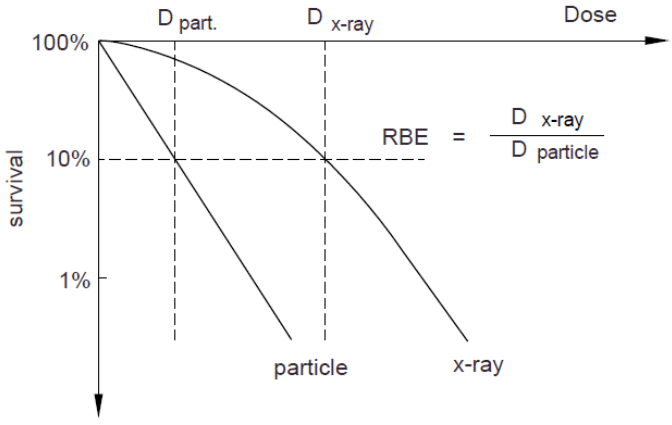

Figure 6: Survival curve with photon shoulder. Definition of RBE, illustrated for cell survival curves. Figure from[29]. The X-ray curve represents low-LET radiation and the particle curve represents high-LET radiation.

Different treatment modalities such as proton and photon therapy are clinically used to treat tumors. Although universally applicable plan parameters for biological effect are desirable, dosimetry is still used to determine the clinical outcome of external beam therapies. Since there is a difference in biological effectiveness between the modalities, this must be taken into account when comparing treatment plans. Up to the present day, the RBE of protons compared to high energy photons is set constant to 1.1. This value was determined *in vivo* during the early days of proton therapy and neglects dependency on dose, endpoint and beam properties[31]. However, much higher RBE values of protons are reported in the distal millimeters of the range[32]. As RBE is defined based on the biological effect, it follows from Formula (7) that it depends on fraction dose, cell type, type of radiation and LET. There is a large spread in RBE data due to inconsistency in experimental design and uncertainty in dosimetry[33]. As the uncertainty in RBE values from experimental data is too large, there is a need for well defined quantities that can predict biological response. If we assume fraction dose, cell type and type of radiation do not change with the range, the increasing RBE at the distal millimeters of the range can in a first approximation be related to the LET of protons.

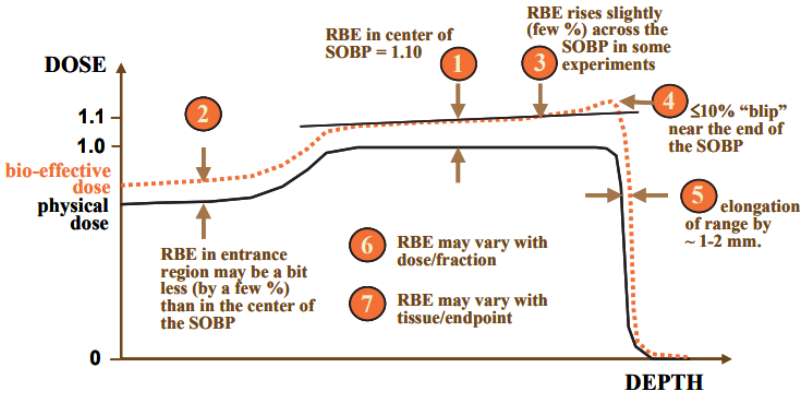

Figure 7: Schematic figure of how the proton RBE can vary from the fixed RBE of 1.1[34].

Both the increase in the distal part of the Bragg peak and the elongation of the range as shown in Figure 7 can be attributed to the increase in LET. The LET is a defined physical quantity, if the relation between RBE and LET is known the LET can be used as a biological predictor. Paganetti *et al* (2019)[33] proposes an RBE vs LET curve, determined under standard conditions at a select number of facilities with small number of human control cell lines.

1.3 Monte Carlo simulations

Monte Carlo (MC) simulation is a numerical approximation method based on the sampling of random objects or processes[35]. The method consists of repeated random sampling from probability distributions. Using the Law of Large Numbers, Monte Carlo simulations provide quantities of interest from complex models and deterministic systems. This approach can be exploited for dose calculations by modeling the physical interactions of a proton traversing a medium. Because of the sharp distal

dose fall-off, small errors in proton dose calculations can be the difference between a volume receiving all of the prescribed dose and receiving none of it[36]. Monte Carlo simulation offers the best results for dose calculation and is used as a benchmark for other dose calculation algorithms such as pencil beam algorithms. This is because MC simulations take the physics of particle interaction into account using theoretical models and experimental data for electromagnetic and nuclear interactions, where pencil beam algorithms rely on kernels in density scaled materials[37].

The MC code that will be used in this study is TOPAS[36]. The TOPAS MC platform is developed because previously available MC codes for proton therapy were underutilized due to their complexity. TOPAS is a user-friendly tool layered on top of the Geant4 toolkit[38]. Geant4 is specially designed for particles passing through matter. Therefore it is a suitable program for the purposes of this study. It is used in particle physics, nuclear physics, accelerator design, space engineering and medical physics. In TOPAS it is possible to model both a passive scattering and scanning beam nozzle and model on CT images. TOPAS can score dose, energy, fluence, LET and also save and restart a phase space. The LET can be track or dose-averaged. LET in TOPAS is scored step-by-step using the kinetic energy of a proton at the beginning of each step using the unrestricted electronic stopping power. The energy is then divided by the step-length to calculate the LET per step. The LET_d per voxel is obtained by multiplying the LET of each step with the energy deposited in that step. The sum of all these products is then divided by the total energy deposited in that voxel to calculate the LET_d. The result is shown to be dependent on the chosen maximum step-length. In general, larger step sizes give faster performance, but smaller step sizes may give better accuracy.

1.4 Dosimetry

Quantifying biological effect as a result of radiation exposure requires accurate dose determination. Absolute dosimetry is needed to determine the deposited dose to the target. There are three main detector types to measure absolute dose: calorimetry, fluence and ionization based. Thanks to its negligible dependence on the energy and LET of a particle, the ionization chamber is the most used detector in particle therapy[39]. In an ionization chamber the average dose-to-air can be calculated by measuring the ionization inside the chamber, together with the mass inside the chamber and the energy required to produce an ion pair in air. Subsequently the dose-to-water is calculated via the Bragg-Gray cavity theory. The Bragg-Gray theory relates the dose deposited in a cavity (usually a gas) to the dose that would be delivered to a medium in case the cavity would not be there.

In this study a large electrode multi-layer ionization chamber (Giraffe, IBA Dosimetry) is used to measure the water equivalent thickness (WET) of our sample-holder components. The Giraffe is specially designed for single-shot Bragg peak measurements. It consists of 180 chambers with 2 mm pitch. By applying the Bortfeld fit[40], the device is able to calculate the proton range compared to measurements in water with a 0.5 mm accuracy[41]. The general equation for WET is

$$t_w = t_m \frac{\rho_m}{\rho_w} \frac{\bar{S}_m}{\bar{S}_w}, \tag{8}$$

where ρ_w and ρ_m are the mass densities of water and material, and $\bar{S}_w$ and $\bar{S}_m$ are the mean proton mass stopping power values for water and material[42]. Instead of using Formula 8 however, the IAEA (2000)[43] proposed that the WET can be approximated by

$$t_w = t_m \frac{R_w}{R_m} \tag{9}$$

where R_w and R_m are the proton range in water and material. The IAEA TRS 398 code of practice refers to the WET as the product of the actual thickness (in cm) and the material density (in g/cm^3)[44]. Both the approximation in Formula 9 and the product of thickness and density can be used to avoid excessive stopping power calculations.

The IAEA TRS 398 code of practice states that larger ionization chambers, such as the thimble Farmer-type or parallel-plate ionization chambers, should be used for single point dose measurements in the centre of a uniform field[45]. The available detector during this study is the Markus parallel-plate ionization chamber (PTW, Freiburg, Germany). Parallel-plate ionization chambers are made using two parallel metallized foils in a gaseous chamber, with a constant voltage difference applied over them[39]. The output signal is proportional to the number of particles passing through the detector.

The ionization chamber is too large be used during experiments as it does not fit in the sample-holder. Therefore in addition to the dose measurement with the Markus chamber prior to an experiment, radiochromic film will be placed in the set-up during an experiment. The radiochromic film used in clinical application at the Erasmus MC is GAFchromic (Ashland Inc.) EBT3. This film is created for photon dosimetry but has been shown to provide measurements accurate to 2% over doses of 0.2-100 Gy for proton therapy[46]. GAFchromic EBT3 film contains three layers, where the active layer is sandwiched between two clear polyester based layers[47]. The active layer contains a dye that changes color when exposed to ionizing radiation[48]. The change in color is relate to the amount of ionizing radiation it is exposed to.

2 Radiobiological experiments in proton beam therapy: Where to start and how to be relevant

This chapter is originally written as a literature study conducted simultaneous with the design phase of the sample-holder. The literature study report is assessed separately, but is included in this thesis because of its relevance.

To answer the first question described in the introduction, the following information from 19 papers will be extracted and summarized in a table: Cell cultureware, endpoint, phantom material, dosimetry, reference radiation, proton radiation, cell survival model and LET. For the second question review articles, database studies and perspective/opinion articles are analyzed.

2.1 Radiobiological experiments on (sub-) cellular level

Prior to summarizing experiments in proton radiobiology it is important to know how such experiments are conducted. Section 2.1.1 treats a typical experimental setup including the corresponding work flow.

2.1.1 Experimental setup

The experimental process is divided into the following sections: sample preparation, experimental setup (proton and gamma), dosimetry, LET simulations and sample analysis.

Sample preparation: The first step is to choose the sample that will be irradiated, which depends on the desired endpoint. This sample needs to be cultivated or deposited into a housing such as a petri dish, flask, multi-well plate, etc. Most used cultureware for radiobiological experiments are flasks and multi-well plates, shown in Figure 8 Biological samples need careful treatment before, during and after irradiation. Cell cultures for instance are usually submerged in a special medium and incubated at certain temperatures and CO_2 levels.

Experimental setup: The experimental setup can be split into delivery and phantom. In the delivery section is described what proton (PBS, PS) and photon (Linac, nuclide) radiation is used and what the energy or energy range, dose rate, total delivered dose, field size and spot size in air are. In the phantom section is described what type of phantom is used and at what position in the beam path the sample is irradiated (plateau, Bragg peak, etc.). An example of a setup for radiobiological experiments is shown in Figure 9.
Dosimetry: Absolute dosimetry is necessary for the verification of the delivered dose to the sample. In most cases an ionization chamber calibrated according to standards is used for his purpose. Additionally some studies perform relative dosimetry with arrays of dosimeters or radiochromic film.

LET simulations of protons: LET is known to be correlated to RBE which makes it an important physical quantity to address. LET can also be interesting for intercomparison of studies using different beam characteristics. Parameters used for the Monte Carlo calculations should be elaborated on.

(a) **(b)**

Figure 8: Cell cultureware often used in radiobiological experiments. (a) 50mL CELLSTAR T25 Flask. (b) Eppendorf multiwell culture plates

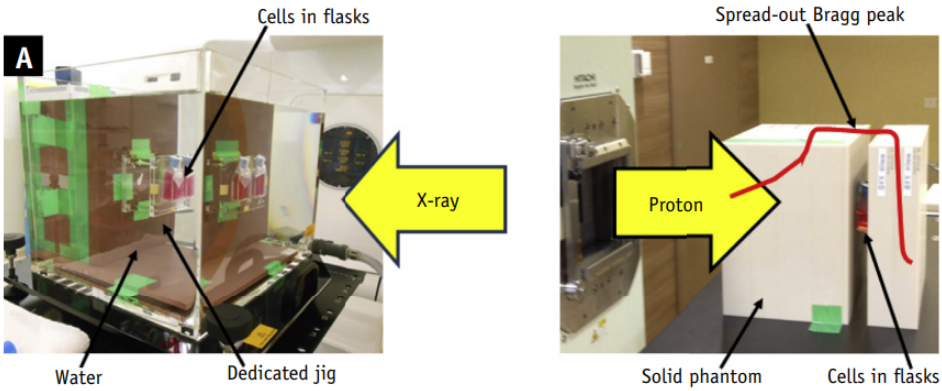

Figure 9: Irradiation method for relative biological effectiveness determination. For X-ray irradiation a water tank is used, for proton irradiation a solid slab phantom is used. Setup and image by Iwata et al.[49].

Sample analysis: Sample analysis depends on the chosen endpoint. For cell survival (so far the most studied endpoint) the standard analysis is clonogenic survival, which is the counting of colonies formed by surviving cells.

2.1.2 Summarizing the data

In this section the applied materials from selected radiobiological studies is summarized. The data of 19 papers is listed in Table 1 and treated per section in the paragraphs below.

Cell cultureware: The component in which the cells are seeded for irradiation, such as a flask or multi-well plate in Figure 8.

With 10 out of 19 studies, the most mentioned seeding unit is a flask filled with medium. Four studies used petri dishes of which one used a 6-well petri-plate. Furthermore two tubes, two chamber microscope slides, one microscope slide and one monolayer are used. As a reason for using a flask filled with medium, Michaelidesová et al. mentions it avoids back scattering and provides the opportunity to irradiate all flasks at once by placing them in a row[50]. An additional advantage of flasks is the possibility of vertical irradiation, in contrast to not completely closed components. Disadvantages of flasks are: high labor intensity when working with larger number of samples and cells prefer to attach to corners and edges, resulting in non-homogeneous coverage.

Endpoint: The endpoint is important for intercomparison of data, as RBE is defined for a certain endpoint (i.e. Surviving Fraction). Intercomparison of RBE values from various experiments using different endpoints is therefore not possible.

14 out of 19 studies use cell survival as their endpoint. This large number is most likely due to the terms used for searching articles. Nonetheless, cell survival will most likely be used as endpoint in the experiments for the thesis that will be conducted and it is therefore good to look at the method used for cell survival measurements. All of the studies that use cell survival as their endpoint apply clonogenic assay. In clonogenic assay, a surviving cell is a single cell with the ability to grow into a colony. Other used endpoints are DNA Double-strand breaks, apoptosis, Foci formation, gH2AX assay, RNA concentrations and single cell gel electrophoresis.

Phantom material: IAEA Codes of Practice TRS-398[44] lists water, PMMA and Polystyrene as possible materials for phantoms in proton therapy experiments.

In 11 out of 19 studies PMMA is used as phantom material. Four studies used a (glycerol)water phantom, two studies used an unspecified solid (water-equivalent) phantom, one study used a cylindrical heater and one study does not mention anything about the phantom material. Explicit reasons for using PMMA as a phantom material are not mentioned in these studies, but are assumed to be the accurate depth positioning, low cost, ease in use and depth reproducibility.

Dosimetry: Dosimetry will be performed during experiments, meaning that it has to be implemented in the design of the sample-holder. How is dosimetry performed in other experiments?

All studies use ionization chambers for reference dosimetry, mostly indicating to do so according to standard protocols. Commonly used protocols for dosimetry are described in IAEA 2000[43], IAEA TRS 398[44], ICRU Report 59[51] and Japanese standard dosimetry 01[52]. In addition to reference dosimetry, nine studies indicate the use of radiochromic film, alanine EPR or an ionization chamber array for relative depth dose profiles and/or lateral dose beam profiles.

Reference radiation: Not all photon radiation has the same radiobiological effect, which makes the choice of reference radiation important in defining the RBE and for intercomparison of data between studies.

Eight out of 19 papers used a Cobalt-60 source as reference radiation. Four used 6 MV photon beams (of which one also used a 4 MV photon beam), four used 220 to 250 kV X-ray beams, one used 10 MV photons, one used Cesium-136 and one used an 120 kV X-ray beam. In none of the papers is explained why that particular type of reference radiation is chosen. It seems appropriate to choose MV photon beams as these beams are used clinically in the Netherlands.

Proton radiation: Proton induced damage depends on the initial energy. Straggling and applying mixed fields for instance result in decreased LET and thus reduced clustered damage. This sections covers whether single Bragg peaks or spread-out Bragg peaks are used in other centers and at what energy they operated.

With the exception of two, all studies used a SOBP. 13 out of 19 SOBPs are created with the minimum and/or maximum modulation energies for clinical use (around 60 to 230 MeV), other SOBPs have energies in between, 87 to 190 MeV. In addition to an SOBP, three studies have also used a pristine BP in their study. One study used a 16 MeV pristine BP in order to yield higher LET values.

Cell survival model: Different studies irradiate with different doses and use different cell types, data from one study can therefore not directly be correlated to the data of another study. By using models to correlate surviving fraction with dose, curves can be fitted to interpolate between data points and retrieve RBE values per surviving fraction or fraction dose.

14 out of 19 studies used the Linear-Quadratic model. Three studies do not mention an RBE model, one used a linear model and one study used a parameterized model based on LET.

LET: Proton RBE is known to be correlated with LET[31], so it is interesting to take LET into account when conducting radiobiological experiments.

In 14 out of 19 cases, the LET is included in the study, of which ten use the dose-averaged LET (LET_D). The remaining four studies that include LET do not elaborate on their LET definition and how this is calculated. Five studies did not include LET in their study.

Table 1: Overview of the materials from listed papers for conducting radiobiological experiments.

First author	Cell seeding for irradiation	Endpoint	Phantom information	Dosimetry	Reference radiation	Proton radiation	Survival model	LET
Petrovic, 2010 [53]	Petri dish (dry, vertical)	Cell survival, proliferation, cycle phase	PMMA	Ion. chamber	Co-60	62 MeV SOBP	LQ	yes
Gerelchuluun, 2010 [54]	Flask and chamber slide	DDSB, Apoptosis, cell survival	Water	Ion. chamber	10 MV	200 MeV SOBP	LQ	LET_D
Calugaru, 2011 [55]	Flask	Cell survival, DDSB	PMMA	Ion. chamber, alanine EPR	Cs-136	76 and 201 MeV SOBPs	LQ	no
Butterworth, 2012 [56]	Flask	Cell survival	Water	Ion. chamber + ion. array	6 MV	101.5–129.46 MeV SOBP	LQ	-
Britten, 2013 [57]	6-well (dish) plate	Cell survival	PMMA	multi-layer ion. chamber	120 kV	87 and 200 MeV SOBP	LQ	LET_D
Sorokina, 2013 [58]	Sterile screw cap microtubes	Foci formation, DDSB	Water	Ion. chambers + electrometer + radiochromic film	Co-60	200 MeV BP	N/A	yes
Slonina, 2014 [59]	Petri dish	Cell survival	PMMA	Ion chamber + 6-sector ion. chamber incl electrometers	6 MV	60 MeV pristine / SOBP	LQ	LET_D
Matsumoto, 2014 [60]	Flask	Cell survival	PMMA	Ion. chamber + electrometer +radiochr. film	6 MV	190 MeV SOBP	LQ	no
Keta, 2014 [61]	Monolayer in medium	Cell viability and cell survival	PMMA	Ion. chambers	Co-60	62 MeV SOBP	LQ	yes
Aoki-Nakano, 2014 [62]	Flask	Cell survival	?	Ion. chambers	4 & 6 MV	180–235 MeV SOBP	LQ	no
Chaudhary, 2014 [63]	Flask	Cell survival	PMMA	Ion. chamber + radiochromic film	225 kV	62 MeV pristine/SOBP	LQ	LET_D
Wouters, 2015 [64]	ABS plastic tube	Cell survival	(Glycerol) Water	Ion. chambers	Co-60	160 & 230 MeV SOBP	LQ	LET_D
Chaudhary, 2016 [65]	Flask	53BP1 foci formation assay.	PMMA	Ion. chamber + radiochromic film	225-kV	60 MeV pristine/SOBP	Param. with LET	LET_D
Cuaron, 2016 [66]	Single chamber microscope slides	gH2AX assay and DDSB	Solid water blocks	NIST traceable chambers	6 MV	152 MeV SOBP	LQ	yes
Iwata, 2016 [49]	Flask	Cell survival	Solid phantom	Electron chamber + ion. chamber	6 MV	225 MeV SOBP(PS), 152.6-200.5 MeV(PBS)	N/A	no
Michaelidesova, 2017 [50]	Flask	Cell survival and micronuclei formation	RW3 PMMA	Ion. chamber	Co-60	181.4-223.1 MeV SOBP	LQ	LET_D
Nielsen, 2018 [67]	Flask	RNA concentrations	PMMA	Ion. chamber	Co-60	low & high-LET proton SOBPs' (11-14 cm)	N/A	LET_D
Panek, 2018 [68]	Precoated microscope slides	Single cell gel electrophoresis (comet) assay	PMMA	Ion. chamber	250 kV	60 MeV SOBP	Linear model	LET_D
Rykkelid, ESTRO37 [69]	Petri dish	Cell survival	Cylindrical heater	Ion. chamber + radiochromic film	220 kV	16 MeV BP	LQ	LET_D

2.2 Performing relevant experiments

Seven recent review articles (from 2018 and 2019) on proton radiobiology are used to determine the current state of knowledge and give an overview of the prospect of various research groups on how to further study proton radiobiology.

Current data that suggests that the RBE of protons is not a constant of 1.1 is so far insufficient to change clinical practice[3]. Contrary to the physical aspects of proton beam radiobiology, the biological aspects (biological endpoints in particular) are not yet well understood. More effort is urgently needed to increase the accuracy of RBE evaluation.

2.2.1 Limitations of current practice

Due to the limited access to proton beams, there is only limited number of samples that can be irradiated which limits the range of parameters that can be studied. Exploiting the so far understudied biological advantages of proton therapy is expected to change clinical practice. If a biological advantage of proton therapy in certain subsets of patients can be determined, this would aid the discussion around the potential of proton therapy[4].

So far only few studies are dedicated to the differential response on molecular and cellular levels between protons and photons[3]. Potential to translate historical data to the clinic is limited by the use of primarily murine tumor cell lines. Two-dimensional cell cultures are insufficient for representing the clinical treatment situation[70].

Neutrons and other secondary particles should be characterized when using range shifters and introducing tissue equivalent material to position biological samples. This is a challenge especially for studies using biological samples placed at or near the Bragg peak, due to positioning and range uncertainty[71].

Clonogenic survival of monolayer cultures from established cell lines is used as endpoint for most available RBE data at the moment. Until now this method is considered appropriate, but its limitations are becoming more evident. The method does not take into account tumor vasculature [72, 73], stimulation of immune responses [74–76], and the impact on tumor response to radiation due to the micro environment[33].

Problems in defining a proton RBE It may be that the RBE of protons is higher than 1.1, especially in the distal millimeters of the Bragg-peak, where it increases with increasing LET. The uncertainty in the increase in RBE is a topic of debate in situations when protons stop near or inside critical structures like the central nervous system [70].

Considering the large amount of data that is available, the spread in absolute RBE values between experiments is remarkable. Inconsistency in experimental design between laboratories and uncertainties in dosimetry may be contributors to a large part of this spread in data. Not only the irradiation conditions between labs are different, so are cell handling protocols. The growth phase, cell densities, time of plating and attachment/suspension are all important factors that affect cell radiation sensitivity[33].

Current RBE estimates depend on the cell type and detection method as it has been

shown that DNA damage and cell death vary between photon and proton irradiation with a.o. tissue type and dose level [77]. Biological differences that cause variability in RBE also include the role of immune responses in vivo[33].

RBE dependence on cell lines/tissue types correlates with their photon fractionation sensitivity of α/β. Systems with a low α/β show a strong decrease of RBE with increasing dose per fraction. Systems with high α/β (10-25 Gy) show lowest RBE values, also below 1.1 [70]. DNA DSB damage after proton irradiation is more complex than after photon irradiation, due to the clustered damage from the higher-LET proton. As the complexity of DNA DSB damage is a factor in the repair pathway choice, this might be an explanation for homologous recombination being the more common repair pathway after proton irradiation, which takes longer to repair DNA than non-homologous end-joining[78].

From experimental data can be concluded that when averaged over all cell lines, RBE for cell survival at 2 Gy per fraction varies from 1.1 in the SOBP entrance, to 1.15 at the SOBP center, to 1.35 at the distal edge of the SOBP and 1.7 at the distal fall-off [31, 66]. This increase in RBE with depth is found to correlate with the increase in LET. RBE thus varies with LET along the path of the beam, mainly near the distal end[70].

In the absence of a reliable RBE model that can be incorporated in treatment planning, other methods should be used. Luhr[70] proposes a four step strategy: (i) Awareness of RBE uncertainty during plan evaluation, (ii) mitigation of the RBE effect during treatment planning to avoid high RBE in critical structures, (iii) generate clinical RBE data using patient outcome data and (iv) initiate clinical in vivo studies. The following RBE mitigation strategies are proposed (a) selection of beam angles and dose reduction in the distal millimeters of the beam, (b) robust optimization and (c) LET optimization.

2.2.2 LET as a surrogate for RBE

Without a RBE model, LET can be a surrogate for RBE. LET_D is a reliable predictor for RBE only in the case of narrow LET distributions but not for broad LET distributions as present in SOBPs and treatment plans[79], this is because the RBE-LET relationship is nonlinear. Articles such as those by Friedrich et al.[80] and Paganetti[31] relate RBE to LET while using experiments with mixed radiation fields. Not distinguishing between SOBPs, pristine Bragg peaks and experiments under track segment conditions result in a scatter of the data. When LET is not linear with RBE, it should not be used as a predictor for biological effect but as a surrogate for varying biological effect[81]. Paganetti et al. propose a "reference" RBE vs LET curve determined under standard conditions at a select number of facilities with small number of human control cell lines. The aim of this curve is standardization of data obtained in future experiments[33]. Standardization of LET vs RBE seems the correct thing to do, as not only experimental set-ups but also calculation algorithms vary between institutes, adding an extra dimension for errors.

Durante et al.[71] address the challenge of LET dependence of dosimeters, which has to be corrected for. LET changes substantially between different regions of the beam path, especially at the distal few millimeters. In order to assess the LET de-

pendent response of dosimeters, Monte Carlo algorithms can be used to simulate the LET distribution of radiation fields. Detailed knowledge of the dose, LET and other physical factors at the point of interest (cell culture plate) is needed. This can be achieved by accurately modeling the experimental geometry i.e. material composition of elements in the beam path in the MC simulation.

Devices are being developed that allow direct LET measurements at micrometer and nanometer scales[79]. These devices may improve our understanding of the biological consequences of proton interactions and ultimately lead to well defined proton specific dose and LET constraints to tumors and organs at risk. Such well defined physical parameters in combination with their known biological consequences can make the RBE as it is now redundant.

2.2.3 Translation to the clinic

Radiation biology research has the goal to translate laboratory findings to clinical practice[71]. Two steps are commonly mentioned: the first step is understanding the biology of radiation response[3, 4, 33], the second is step is for experiments to stay as close to the clinical situation as possible[70, 71].

Understanding the biology of radiation response More sophisticated *in vitro* and *in vivo* models are needed to mimic the heterogeneous tumor structure[70]. Current in vitro experiments are well justified and should be continued, but are insufficient to change the constant clinical RBE. Especially more in vivo studies are needed before RBE variations can be implemented in proton therapy[3].

There is a need for studies to assess the relevance of clonogenic survival as an endpoint for RBE. Paganetti et al. request additional models and/or endpoints to achieve a full understanding of appropriate RBE values. Potentially interesting studies from the biological side are the differences in response to protons and photons of: angiogenesis and cell migration[82], patterns of gene expression [82, 83], DNA methylation[84], and production of ROS [85]. Differences in response for these processes may support a variable RBE in proton treatment planning[19][33].

In vitro and *in vivo* experiments are needed to understand biological damage and repair mechanisms in order to improve characteristics for models such as LEM. Extra care should be taken to the physical characteristics of the beams used for these experiments for better uniformity in laboratory conditions[71].

Molecular mechanisms that contribute to differential RBE values can be understood in more detail using a high-throughput approach[33]. With a high-throughput approach it is possible to assess response at multiple dose levels in a large number of patient-derived cell lines. This large amount of data can then be combined with knowledge of the genomic profiles of each cell line.

Multi-scale models may be capable of characterizing all stages of cellular radiation response[4]. Collaborations between experimentalists and modelers should lead to the design of multi-scale experiments, combining terminal endpoints (cell survival) with quantification of intermediate processes (DNA repair, mutation, chromosome aberrations).

The pipeline in Figure 10 is proposed for the discovery of clinically useful biomarkers to predict variable RBE values[4].

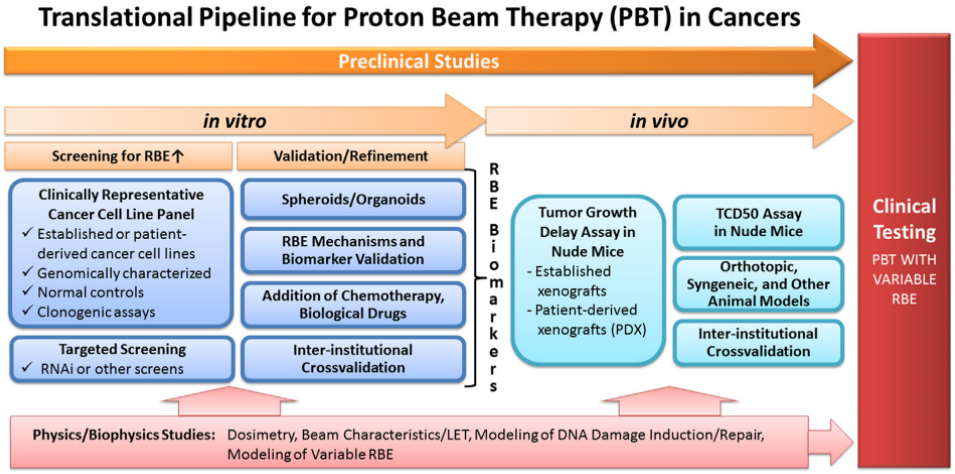

Figure 10: Translational pipeline for proton beam therapy in cancers by Willers et al.[4]

Confining to the in vitro part of the pipeline, experiments are placed in two phases: Screening for RBE and Validation/Refinement. Screening for RBE consists of standardizing clinically representative cancer cell lines with known behaviour by means of a panel and the targeted screening using RNAi or other screens. For validation/refinement the authors propose the use of Spheroids & organoids, RBE mechanisms & biomarker validation, addition of chemotherapy or biological drugs and inter-institutional cross-validation.

Recent findings suggest that DNA repair-pathways such as homologous recombination or the Fanconi Anemia pathway may explain a part of the variation in RBE values found between human tumor cell lines[78, 86, 87]. Besides explaining the differences in proton RBE found in experiments, these deficiencies in repair-pathways can be used in human tumors that suffer these deficiencies and can even be combined with pharmacological agents to even further exploit defects in repair pathways[33]. If a biological advantage of proton therapy in certain subsets of patients can be determined, this would aid the discussion around the potential of proton therapy[4].

Stay close to the clinic Experiments that do get carried out should be coordinated for translation to the clinics. Considerations are among others improving cell culture systems including translational endpoints and the use of a clinical exposure situation. Human pluripotent stem cell-derived 3-dimensional organoid systems may close this gap[88]. Proton beams used for experiments should consist of a clinical composition of energies that cover the entire target with a homogeneous dose[70][71]. Basic physics experiments often use a pristine Bragg-peak or spread-out Bragg peak with non-clinical energies. The difference in number of particles, energy spectra and dose rate per small unit area between passive scattering and active scanning is an important factor to take into account[71].

2.2.4 Intercomparison of data

Intercomparison of data is critical to reduce the spread in values between studies. Detailed reporting of physical parameters and their uncertainties is of great importance for intercomparison of experimental data, this also applies to researchers using clinical beams[71].

Understanding the (biological and physical) reasons for the spread in RBE values is needed in order to improve experimental techniques. Comparison of experimental outcomes between laboratories can be realized by standardization and accurate reporting of experimental and dosimetric procedures [33]:

- Use 6-MV photons or Cobalt-60 as reference photon radiation.
- Potential alternative approximation to proton RBE for the analysis of experimental data is to use proton LET_D relative to LET of secondary electrons from photon reference radiation.
- Provide detailed physics experimental design information including LET_D as it is essential for biological effect models.
- Scanned proton beams have narrower energy spectra compared to scattered proton beams, which is why LET_D spectra of scanned proton beams provide highest quality LET_D data.

Going forward it would be ideal to have a list of minimally available dosimetric information on an experimental setup and a standard set of biology conditions to allow intercomparison of data among labs. The standardization will help reduce uncertainty as well as quantifying the dependence of RBE variability on LET, dose, dose per fraction and tissue/cell type[33].

Durante et al.[71] have constructed a set of parameters and measurements that should be addressed when publishing on pre-clinical radiobiology of heavy ions: Irradiation technique, Fluence calibration, Physical dose, Time structure of the beam, Fluence at multiple time scales, Dose rate, Dose and fluence spatial uniformity, Nominal ion species, Ion beam purity, Nominal beam energy, SOBP width, Particle spectrum, LET for each ion or microdosimetric spectrum, List of beam modifiers and their characteristics. A more detailed description of the parameters including methods, suggested reporting and desired accuracy is described in the article. Personally I think a standard set of parameters and measurements is very useful to have when designing an experiment, in addition to allowing intercomparison it also acts as quality assurance.

2.3 Conclusions

The topics raised for this literature study are on how to conduct radiobiological experiments at cell level and how to be relevant with the conducted experiments. This is what can be concluded:

Radiobiological experiments at cell level: According to Table 1, an experimental setup to perform radiobiological experiments on cell level is conducted as follows: The endpoint is cell survival and the cells are irradiated in a flask or a 6-well plate, surrounded by a PMMA or water phantom. Absolute dosimetry is performed with an ionization chamber and can be complemented with relative dosimetry using radiochromic film. As proton irradiation a SOBP is used, reference radiation can be a

Cobalt-60 source, 6 MV photons or 200-225 kVp X-rays. Sample analysis is performed by means of clonogenic survival. The linear-quadratic model for fitting a cell-survival curve and dose-averaged LET calculations can be conducted for intercomparison of data.

How to perform relevant experiments: There is a large spread in RBE data due to inconsistency in experimental design and uncertainty in dosimetry. Better understanding of radiation response is needed, for which multi-scale experiments and high-throughput approaches are proposed. To really contribute to proton radiobiology it is important to conduct experiments in such a way that the acquired data can be translated to the clinic and can be compared and/or combined with data from other centers. Experiments should have accurate reporting, minimum dosimetric information and a standard set of parameters and biological conditions.

3 Materials and Methods

The objectives of this thesis are to design a sample-holder, work out the dosimetry and perform radiobiological experiments with it. In addition Monte Carlo LET calculations are performed based on the characterization of a Bragg peak in the setup.

3.1 Sample-holder design

Many considerations have led to the final design of the sample-holder: cultureware, material, position accuracy & stability during handling, ease in use and use of dosimetry during the experiment. In this study the most important of these considerations is the cultureware, as our choice of cultureware brings additional challenges. The cells are provided by the Molecular Genetics department of the Erasmus Medical Center, who prefer 6-well plates as cultureware because they are easy use and the uniform distribution of cells on the bottom of the wells.

Future experiments will be conducted in the Holland PTC research bunker, which has a fixed horizontal beamline. As the 6-well plates are not completely closed, fluids will leak out when positioned vertically. Because the 6-well plates cannot contain any liquids in this position, the cells will be irradiated without the culture medium which provides them the necessary nutrients, growth factors and hormones and that regulates the pH and osmotic pressure[89]. The culture medium needs to be removed prior to the experiment and new medium should be added directly after the experiment. The maximum time for cells to be unaffected by the lack of culture medium is expected to be 5 minutes. This time window requires the 6-well plate to be inserted and removed quick and easy without changing the position of the sample-holder.

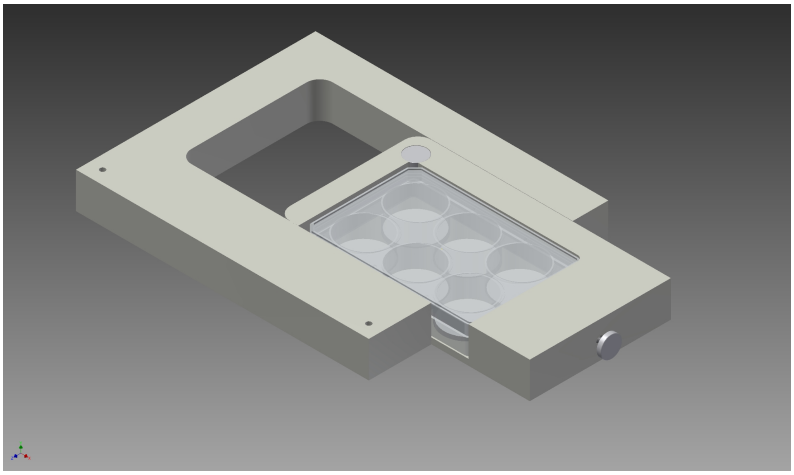

Figure 11: Custom designed drawer system as part of the sample holder. The system allows quick and easy insertion and removal of the 6-well plate. Courtesy of Roel Hoogeveen

As suitable materials for phantoms in proton therapy experiments, the IAEA Codes of Practice TRS-398[44] lists water, PMMA and Polystyrene. Often solid water "RW3"

phantoms are used, which consists of polystyrene slabs with a mixture 2.1% TiO_2[90]. However due to the added Titanium, RW3 is not recommended to use in proton therapy. Because the 6-well plate is not completely closed, a water tank is not suitable as sample-holder. Based on fabrication costs and availability, polystyrene is chosen as material for this sample-holder. Ten slabs with a thickness of one centimeter can be stacked on top of each other, connected with two pins to fix their position relative to each other as shown in Figure 12. In addition the choice is made for: one slab of 5

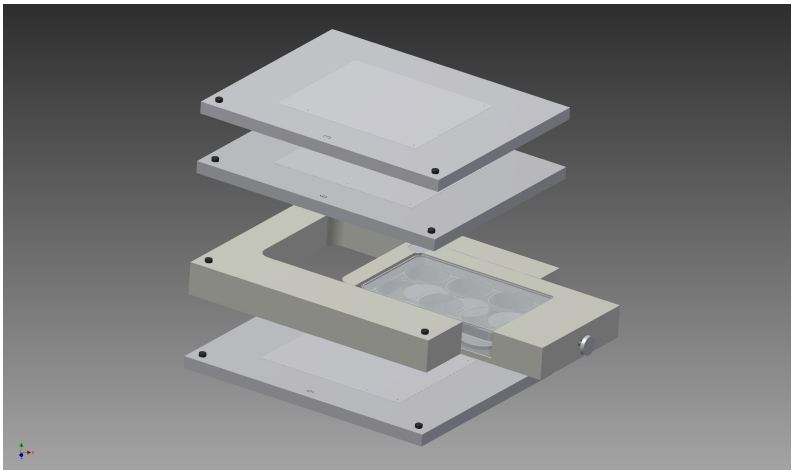

Figure 12: Stacking of polystyrene phantom. Courtesy of Roel Hoogeveen

millimeter, four slabs of 1 millimeter and one slab of 0.5 millimeter, in order to vary the build-up thickness for different proton energies. The 6-well plate is placed in a 2.5 cm thick slab with a 'drawer' system as shown in Figure 11. The drawer allows for quick and easy handling of the 6-well plate when time is a limiting factor.

Dosimetry during the experiment is performed using radiochromic film, which can be placed between two slabs. Position reference of the radiochromic films is done by punching small holes on three corners using a pushpin. Accurate punching is guaranteed using an additional 'punching'-slab with three holes the size of the pushpin. Every slab contains three small wells on the same positions as the punching-slab to allow the pushpin to penetrate the film.

3.2 Dosimetric validation of the sample-holder

In order to create a dose plan for the sample-holder, it needs to be dosimetrically characterized. First the WET and thickness uniformity of the slabs will be measured. Subsequently radiochromic film will be used for spot characterization and range verification. Finally radiochromic films will be calibrated for absolute dosimetry using a PTW Markus chamber.

3.2.1 WET measurements

WET measurements are needed for reliable dose calculations. WET measurements are perfomed in order to calculate the density. Because the slabs of 10 and 5 mm

thickness have the same manufacturing process they are considered the same material. WET measurements are therefore only performed on a 10 mm thick slab. This the same for 1 and 0.5 mm slabs, where only the WET of a 1 mm slab is measured. Also the WET of the drawer system (as shown in Figure 11) and the bottom of the well & lit of the 6-well plate will be measured. Thickness uniformity is determined by measuring the WET at five positions of a 10 mm slab. WET dependence on the energy is analyzed by irradiating a 10 mm thick slab with five different energies: 70, 110, 150, 190 and 230 MeV. WET measurements are performed with the IBA Giraffe

Figure 13: Setup for the WET uniformity measurements, the targets are placed in front of the IBA Giraffe.

by placing targets in front of its entrance as shown in Figure 13. The targets are irradiated with a 150 MeV single pencil beam (ProBeam system, Varian). The WET is calculated by comparing the R_{80} with and without target positioned in front of the Giraffe, where R_{80} is the depth at which the absorbed dose beyond the Bragg peak falls to 80% of its maximum value[91].

3.2.2 Dosimetry using radiochromic film

Radiochromic EBT3 film is calibrated to a PTW Markus ionization chamber (which is calibrated as a secondary standard) in order to use the film for absolute dosimetry and for spot characterization and range verification.

Absolute dosimetry will be performed using the RW3 phantom because this phantom has specially designed slabs to fit the ionization chamber. To check whether the dose deposition in the RW3 phantom is different compared to our polystyrene sample-holder, the measurement will be performed with both RW3 slabs and polystyrene slabs above the film as shown in Figure 14.A. The film is placed directly on top of the ionization chamber to have the measurement points coincide as much as possible. The color change of the radiochromic film is calibrated to the measured dose with the ionization chamber. The same box plan as used for clinical quality assurance (QA) will be used for this experiment, which is a 10x10x10 cm field, centered at a depth of 10 cm (calculated for RW3). It is known from these QA procedures that the dose

delivered to the RW3 phantom is constant over time. It is expected that the dose delivered to the polystyrene phantom will be the same as to the RW3 phantom.

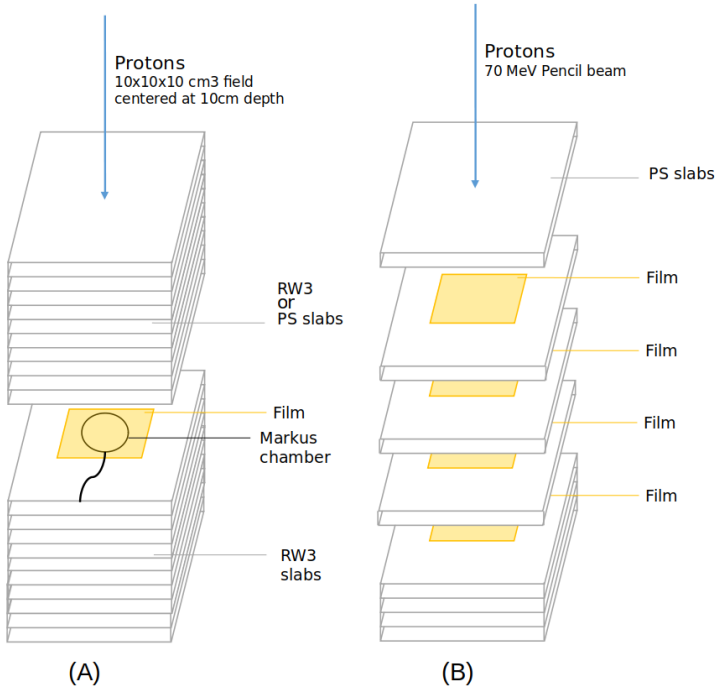

Figure 14: Measurement setups for (A) Absolute dosimetry calibration for EBT3 radiochromic films and (B) Spot characterization and depth-dose reconstruction in the PS sample-holder using EBT3 radiochromic film.

Range verification and spot characterization is done by placing EBT3 film between every slab along the path of the protons. The sample-holder is stacked as in Figure 14.B with films at the following depths: 1 cm, 2 cm, 3 cm, 3.5 cm, 3.7 cm, 3.9 cm and 3.95 cm. The phantom is irradiated with a 70 MeV single pencil beam with 3300 MU at a rate of 100000 MU/min. The films are scanned, relative dose will be measured and will be compared to calculated doses with TOPAS and RayStation.

3.3 Monte Carlo LET calculations

Dose-averaged LET values are retrieved from TOPAS 3.2.0/Geant4 10.05.p01. TOPAS calculates LET based on methods discussed in two papers on LET in Geant4[92, 93]. The sample-holder shown in Figure 15 is modeled in TOPAS using the basic geometries TsBox and TsCylinder. In Figure 16 the same simulation is shown, but with 100 proton tracks visualized.

A custom material is created based on the chemical composition (C8H8, weight fractions H=0.077418 and C=0.922582) and mean excitation energy (68.7 eV) from the NISTdatabase[94] and the density (1.041 g/cm^3) calculated from the WET measurement. The proton source is modeled as a flat, rectangular source of 12.5 cm by 16.5 cm. The number of 10^7 particles is used in this simulation. LET is scored in

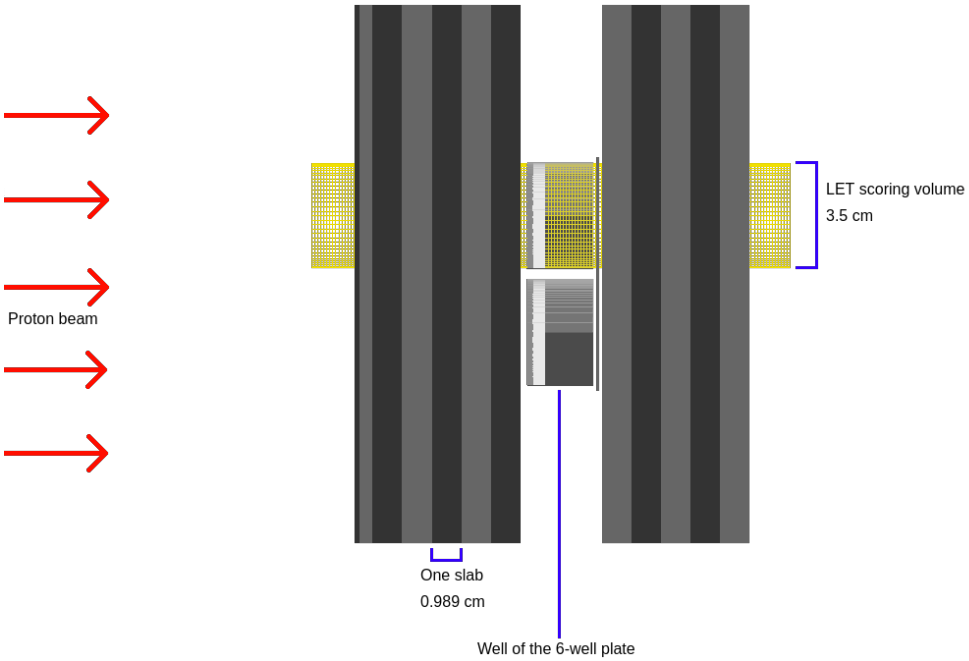

Figure 15: Side view of the sample-holder geometry from the TOPAS MC simulation.

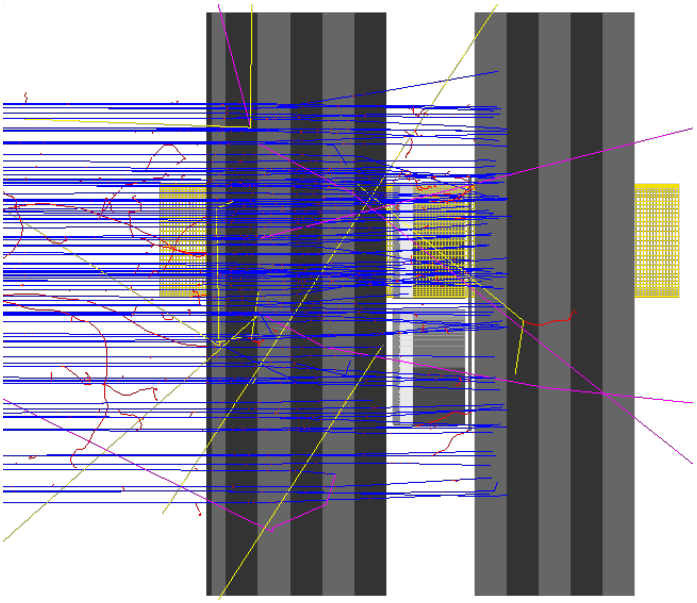

Figure 16: The same side view as in Figure 15, but with 100 particle tracks of two proton energy layers (89.50 and 92.20 MeV) visualized. The shown particles are protons (blue), electrons (red), gammas (yellow) and neutrons (magenta).

a 16 cm long cylinder visible in Figure 15 in yellow. The radius is 1.75 cm which is identical to the well diameter. The LET scoring bin size is 1 mm, the maximum step length (the length that a particle travels between two interactions) is 0.2 mm in the bottom of the well and in the medium and 1 mm (default) elsewhere. The maximum step limit in the well-bottom and medium is based on the scoring bin size. The step limit in the bottom of the well and the medium is different to the rest of the sample-holder, as that is the region where we want to calculate LET values in. Using larger step-limits in the rest of the phantom saves calculation time. Additional restrictions to save calculation time are the minimum electron production threshold of 0.05 mm (range in matter, production energy threshold is different per material) and neglecting secondaries generated in medium with a density below 0.01 g/cm^3.

3.4 Radiobiological experiments

Cell survival experiments are performed to confirm that the sample-holder is suitable for radiobiological experiments. There is a risk of not hitting cells in the Bragg peak due to calculation errors. Therefore, cell survival curves will therefore be constructed for irradiation in the plateau region as well as in the Bragg peak. Figure 4 shows that in the plateau region, a slight miscalculation of the range of several millimeters will result in only a 1% change in delivered dose and LET. Dose delivery is checked by placing EBT3 film underneath the 6-well plate. If the range calculation is correct, irradiation of cells in the Bragg peak enables the comparison of cell survival between exposure to different LET levels. This is because the LET of protons is significantly higher in the Bragg peak compared to the plateau region, see Figure 4 in Section 1.1.1.

The experiments with protons are conducted in a clinical gantry, using a vertical beam. Future experiments however will be conducted in the research beamline, which only has a horizontal beam. When irradiating with a horizontal beam, the 6-well plates have to be placed in a vertical position. As the 6-well plates used for these experiments are not completely closed, these wells cannot contain medium during irradiation in a horizontal beamline. This opportunity of irradiating with a vertical beamline is used to study the difference of cells being submerged in medium versus cells where the medium is temporarily suctioned (5-10 minutes). As shown in Figure 17, three wells per irradiation will contain medium and three wells will not. Results will show whether cells are affected by the lack of medium during irradiation. The proton therapy facility is not yet equipped with an incubator, causing the cells to be exposed to room temperature for five hours during transport and irradiation. To study the effects of cells being exposed to room temperature for that long, additional experiments are performed with photons. Identical experiments will be conducted for cells that have been incubated and cells that are exposed to room temperature for five hours. During photon irradiation the 6-well plates contain three wells with medium and three without, just as in the proton experiments.

3.4.1 Sample preparation

Nine 6-well plates are used for proton irradiation, five plates for irradiation of cells in the plateau region and four plates for irradiation in the Bragg peak. Human bone osteosarcoma epithelial cells (U2OS) are chosen because of their ability to withstand unfavorable culture conditions. The cells were cultivated by the Molecular genetics department of the Erasmus Medical Center, Rotterdam. Cells were seeded in 6-well

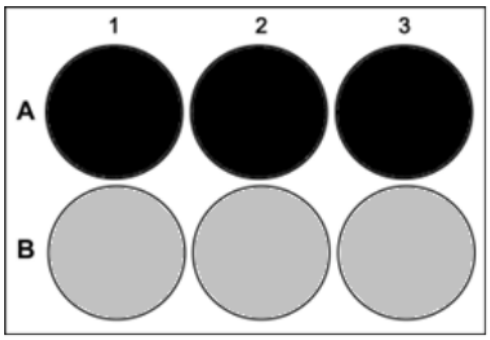

Figure 17: Layout of the 6-well plate during irradiation. The black colored wells A1, A2 and A3 will contain medium during irradiation. The grey colored wells B1, B2 and B3 will not contain medium during the experiment

plates with a density of 400 cells per well, growing in DMEM (Dulbecco's modified eagle medium) medium with 10% FCS (fetal calf serum) and added penicillin/streptomycin. Cells are incubated overnight at 37°C and 5% CO_2. Cells were transported to the proton facility one hour before irradiation.

3.4.2 Irradiation

The irradiation procedures for photon and proton irradiation are discussed separately in the paragraphs below.

Proton irradiation
Dose plans are made in RayStation 7 (RaySearch Laboratories, Sweden) and irradiated with a clinical gantry of a ProBeam® Pencil beam scanning system (Varian Medical Systems, Inc.) at Holland PTC. To model the sample-holder in RayStation, a CT scan of an existing phantom is used with a density overwrite according to the results of the WET measurements. Plans are generated as a homogeneous field with a maximum deviation of ± 2% of the planned dose. Plans are made with a 2 cm margin on all sides of the target to ensure full coverage of the target. The plans for irradiation in the plateau region are made using a single energy layer of 150 MeV protons, see Figure 18.a for the depth dose curve. Cells are placed at a depth of 3.60 g/cm^2 and irradiated with doses of 0.45, 0.91, 1.82, 2.73 and 3.64 Gy. The plans for irradiation in the Bragg peak are made using two energy layers of 89.50 and 92.20 MeV, which together cover the layer of cells, see Figure 18.b for the depth dose curve. Cells are placed at a depth of 5.79 g/cm^2 and irradiated with doses of 0.91, 1.82, 2.73 and 3.64 Gy.

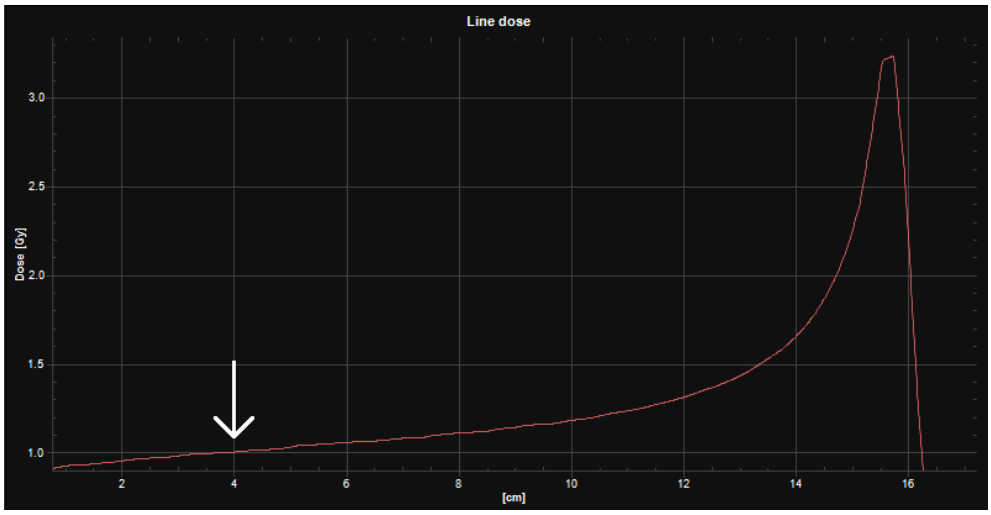

(a)

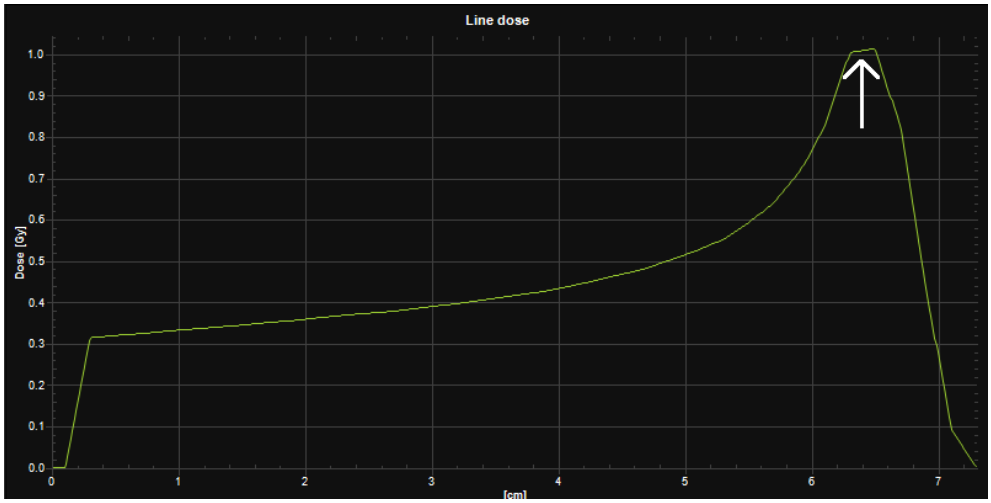

(b)

Figure 18: Depth dose curves for large irradiation fields using (a) a 150 MeV field and (b) a combination of 89.50 and 92.20 MeV. White arrows indicate the position of the cells for the radiobiological experiment experiments.

It is desirable to leave the cells without medium as short as possible. To do so, medium is extracted and added inside the irradiation room just before and after irradiation. EBT3 film with equal size of a 6-well plate is placed underneath the 6-well plate as that is the closest position to the cells, as shown in Figure 19. New medium is pipetted in the three wells after irradiation and the EBT3 film is stored in a dark place.

Photon irradiation

Photon irradiations were performed with a RS320 X-Ray research irradiator cabinet (Xstrahl Limited, Surrey, UK) in the Erasmus Medical Center, Rotterdam. 6-well plates are placed in the cabinet and irradiated with 1, 2, 3 and 4 Gy. The dose rate

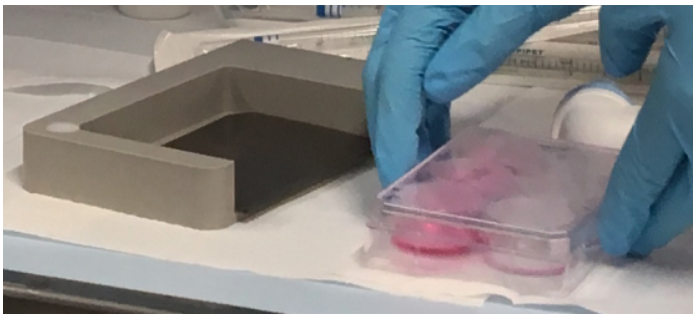

Figure 19: 6-well plate and EBT3 film after irradiation, ready to add new medium to exposed cells.

is constant while irradiation times depend on the dose. The cabinet is set at 195 kV and 10 mA and the dose rate is 1.67 Gy/min.

3.4.3 Analysis

Cell survival analysis is done by means of clonogenic assay. For every irradiation situation there is one non-irradiated 6-well plate that serves as control. From the clonogenic survival data of eight different conditions, the following cell survival curves will be constructed:

X-ray irradiation

- Cells that were on room temperature for five hours and were irradiated with medium (Ph/RT/Med)
- Cells that were incubated and irradiated with medium (Ph/37/Med)
- Cells that were on room temperature for five hours and were irradiated without medium (Ph/RT/Dry)
- Cells that were incubated and irradiated without medium (Ph/37/Dry)

Proton irradiation

- Cells that are irradiated in the Bragg peak, with medium (Pr/BP/Medium)
- Cells that are irradiated in the plateau region, with medium (Pr/Pl/Medium)
- Cells that are irradiated in the Bragg peak, without medium (Pr/BP/Dry)
- Cells that are irradiated in the plateau region, without medium (Pr/Pl/Dry)

Analyzing the curves gives insight into the biological effects on cell level of the conditions that cells were exposed to: being on room temperature for five hours, having no medium for 5-10 minutes and irradiation in the proton Bragg peak vs plateau region. For cells that were irradiated in the proton Bragg peak vs plateau region, cell survival numbers may be linked to the calculated LET values.

4 Results

The results of the WET measurements, film dosimetry, Monte Carlo LET_d calculations and cell survival experiments are presented in this chapter.

4.1 WET measurements

The WET values of the irradiated targets are listed in Table 2. The WET is a direct result of the measurements, the density [g/cm^3] is the WET multiplied by the density of water and divided by the thickness of the target.

Table 2: Water equivalent thickness (WET) measurements of five targets, used for range calculations in dose planning.

Target	**WET [cm]**	**Density [g/cm^3]**
10 mm polystyrene slab	1.03	1.04
0.5 mm polystyrene slab	0.05	1.06
Drawer slab	0.42	
6-well plate bottom	0.13	-
6-well plate bottom + lit	0.24	-

The density of a 10 mm thick slab is 1.04 g/cm^3 and the density of a 0.5 mm polystyrene slab is 1.06 g/cm^3. These density values will be used for range calculations in RayStation and TOPAS MC. The density measruement of the 10 mm thick slab will also be used for the 5 mm thick slab and the density of the 0.5 mm thick slab will also be used for the 1 mm thick slabs.

The thickness uniformity of a 10 mm thick polystyrene slab is measured as the WET on five different positions as shown in Figure 13. The results are shown in Table 3.

Table 3: Water equivalent thickness (WET) uniformity measurement on five positions on a single polystyrene slab of 10mm. Measured with at 150 MeV single pencil beam. Positions correspond to the numbers in Figure 13.

Measurement	**WET [cm]**
Position 1	1.03
Position 2	1.03
Position 3	1.03
Position 4	1.02
Position 5	1.03
Mean	1.03
SEM	0.002

The mean WET is 1.03 g/cm^2 and the standard error of the mean (SEM) is 0.002 g/cm^2. The results of the energy dependency measurements are listed in Table 4.

Table 4: WET dependence on the initial energy of protons.

Energy [MeV]	WET [cm]
70	1.04
110	1.03
150	1.03
190	1.03
230	1

The WET decreases with increasing initial proton energy. The WET is constant for 110-190 MeV protons and decreases from 1.03 to 1 from 190 to 230 MeV.

4.2 Dosimetry using radiochromic film

A large homogeneous box plan is used to irradiate both the RW3 phantom and the polystyrene phantom. The dose is measured with an ionization chamber as well as EBT3 film, as shown in Figure 14. The hypothesis is that the delivered dose (as measured with the Markus ionization chamber) and measured dose with EBT3 film is the same for both phantoms. The delivered doses and measured doses with the EBT3 film are listed in Table 5.

Table 5: Absolute dosimetry calibration of EBT3 film with a Markus ionization chamber

Measurement	Delivered dose [Gy]	Measured dose [Gy]
0 Gy, control	0	0.28
2 Gy in RW3	1.984	2.00
4 Gy in RW3	3.963	3.98
2 Gy in PS	1.976	2.20

The delivered dose and the measured dose for the 2 Gy and 4 Gy irradiations in the RW3 phantom agree within 1%. In the polystyrene phantom however, there is a difference of 11% between the delivered dose and measured dose for the 2 Gy irradiation.

A 70 MeV single pencil beam is shot at the polystyrene phantom with EBT3 films placed between the slabs. Relative doses along the central axis of the pencil beam are obtained by measuring the dose at the center of the spots on the films, see Figure 20.

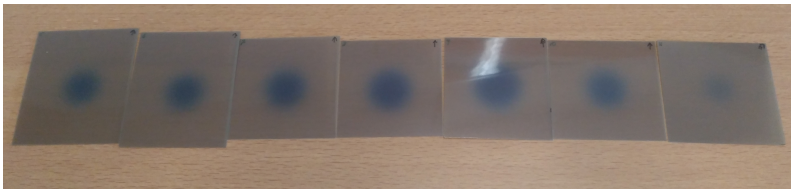

Figure 20: EBT3 radiochromic film irradiated with a 70 MeV single pencil beam. Depth increases from left to right, see Table 6. The films have a size of approximately 3-4 cm per side

The goal was to reconstruct a Bragg peak by placing 7 films along the depth. The films were placed at pre-calculated depths from which we expect to be able to reconstruct

the Bragg peak. From left to right, the films in Figure 20 are ordered from most shallow to deepest. The relative doses for every depth are listed in Table 6.

Table 6: Normalized dose values from a 70 MeV single pencil beam irradiation per depth in Polystyrene

Depth [cm]	Normalized dose
0.99	0.28
2.01	0.32
3.03	0.43
3.52	0.60
3.78	1.00
4.01	0.29
4.09	0.07

The central axis doses of a 70 MeV single pencil beam are calculated using RayStation and TOPAS MC and are plotted in Figure 21 together with the measured doses from the EBT3 films.

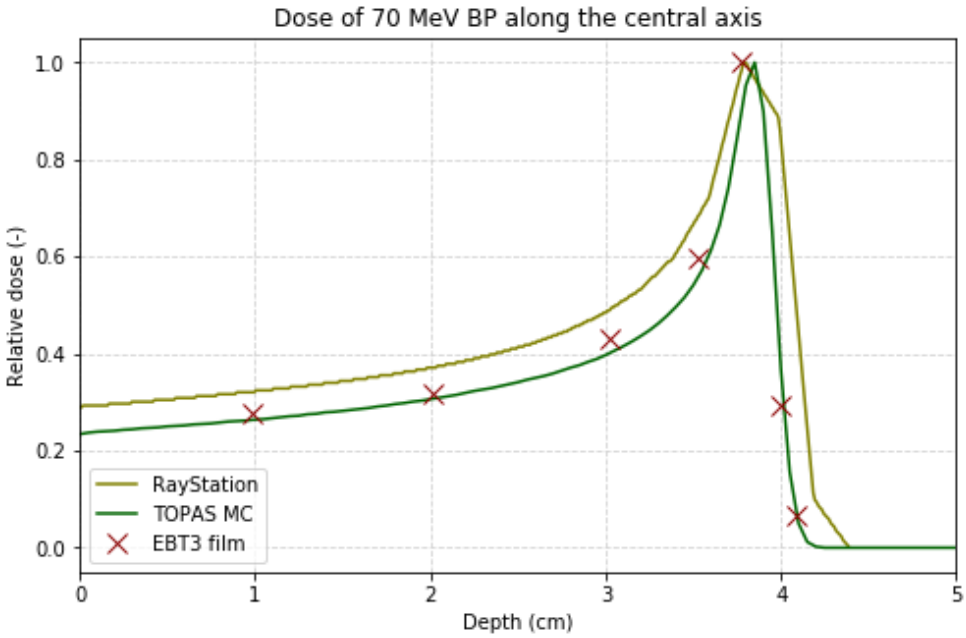

Figure 21: Normalized depth dose profiles of a 70 MeV single Bragg peak along the central axis. Calculations in RayStation and TOPAS MC are plotted together with measured values using EBT3 radiochromic film.

It can be seen that the measured doses with the EBT3 film are up to 20% lower compared to the calculated doses using RayStation. The measured doses are up to 5% higher compared to the calculated doses using TOPAS MC. The Bragg peak calculated in RayStation has a larger distal penumbra than the Bragg peak calculated in TOPAS. The depth-dose curve calculated in TOPAS agrees better with the doses measured with EBT3 film, both in depth and intensity. Remarkable is that the distal

fall-off of the curve calculated in RayStation is spiked compared to the rest of the curve.

By normalizing all curves to their maximum value, the reader may be biased by thinking that the maximum measured value with EBT3 film is the position of the Bragg peak. However, the EBT3 film that received the highest dose was not necessarily positioned in the Bragg peak. Its actual Bragg peak may be shallower or deeper. Additional scaling of the dose (not the depth) is performed based on the doses in the plateau region and proximal part of the Bragg peak. This is the region where less variation in dose is expected due to different calculation methods. The results are shown in Figure 22.

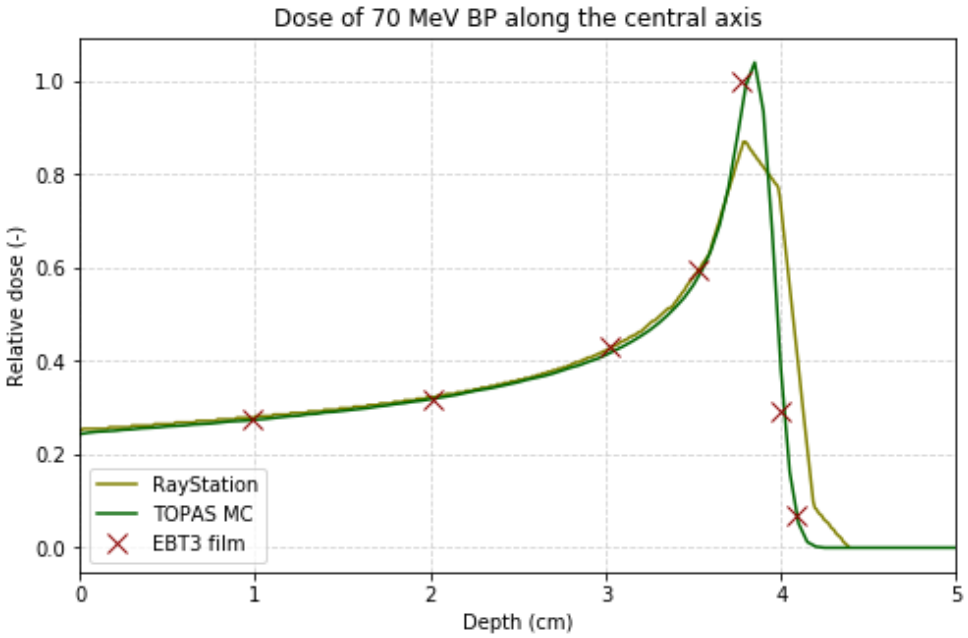

Figure 22: Depth dose profiles of a 70 MeV single Bragg peak along the central axis with scaled doses. Calculations in RayStation and TOPAS MC are plotted together with measured values using EBT3 radiochromic film.

It can be seen that the calculations by RayStation and TOPAS now agree better with the measured doses. The dose calculation from TOPAS agrees within 1% with the measured dose values along the whole depth, including the distal fall-off. The calculation from RayStation agrees with the measured doses in the plateau region and proximal part of the Bragg peak, but differs with 15% in the Bragg peak and over 100% in the distal fall-off.

4.3 Monte Carlo LET$_d$ calculations

LET$_d$ values are calculated in TOPAS for the proton plans made for radiobiological experiments. The proton energies and experimental setup were modeled in TOPAS according to the actual radiobiological experiment. The LET$_d$ values are scored in the

geometry that resembles the density and volume of the culture medium (see Figure 15 in Section 3.3) and are listed in Table 7.

Table 7: Dose averaged LET (LET_d) values at cell depth for irradiation in the plateau region of a 150 MeV uniform field (see Figure 18.a) and in the Bragg peak of a 89.50 & 92.20 MeV uniform field (see Figure 18.b), calculated in TOPAS MC.

Cell location	**LET_d [keV/μm]**
Plateau	1.30
Bragg peak	3.78

From Table 7 it can be seen that the cells that were irradiated with the Bragg peak plan were exposed to an almost three times higher LET_d compared to cells that were irradiated with with the plateau region plan.

4.4 Cell survival experiments

Cells are irradiated with protons and X-rays, under different circumstances. With protons, cells were irradiated in the plateau region and in the Bragg peak. Both in the plateau region and in the Bragg peak there were cells with medium and without medium (dry) in the well. Clonogenic survival after proton irradiation is shown in Figure 23.

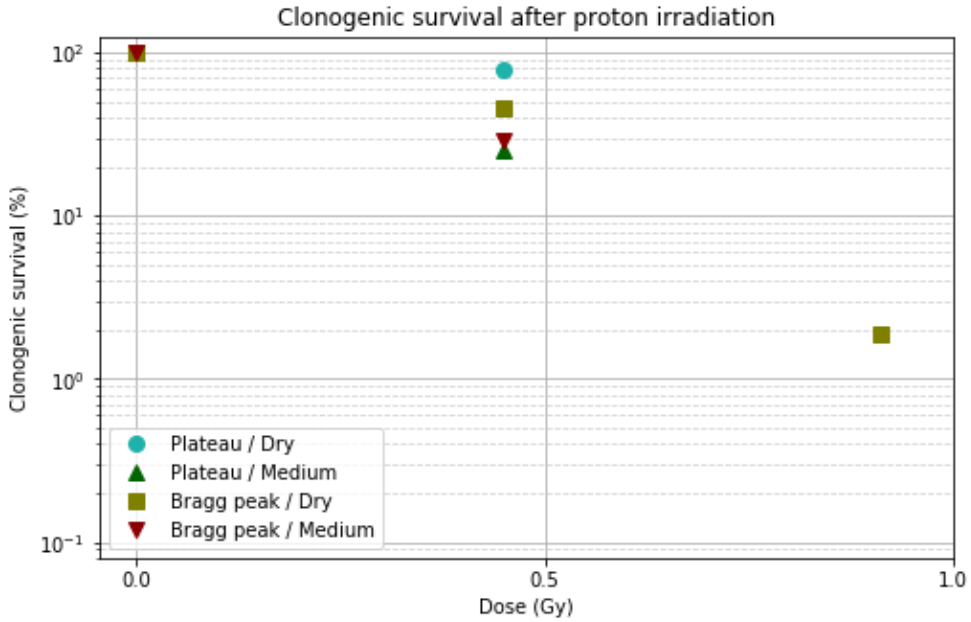

Figure 23: Clonogenic survival of U2OS cells after proton irradiation. Every marker is the average surviving fraction of three wells. Cells were irradiated in the plateau region of a single energy layer (150 Mev) or in the two-layer Bragg peak (89.50 and 92.20 MeV), both large fields covering the whole 6-well plate. For both positions, cells with medium and without medium (dry) were irradiated.

Although cells were irradiated up to 3.64 Gy, Figure 23 shows that there is no colony

formation after 0.91 Gy. Only the cells that were irradiated in the Bragg peak and without medium in the well were able to form colonies beyond 0.45 Gy. Because of this limited amount of data, no linear-quadratic curves are fitted. Although preliminary, from the 0.45 Gy data it can be seen that irradiation in the Bragg peak results in more cell death compared to irradiation in the plateau region. In addition to this, cells that had medium in the wells during irradiation formed less colonies than cells that had no medium in the wells.

Figure 24 shows clonogenic survival after X-ray irradiation for cells that were at room temperature for four hours and cells that were incubated. Just as with the proton irradiations, there were cells with medium in the well and without medium (dry) in the well. Linear-quadratic curves are fitted on the data and the corresponding α and β values are given.

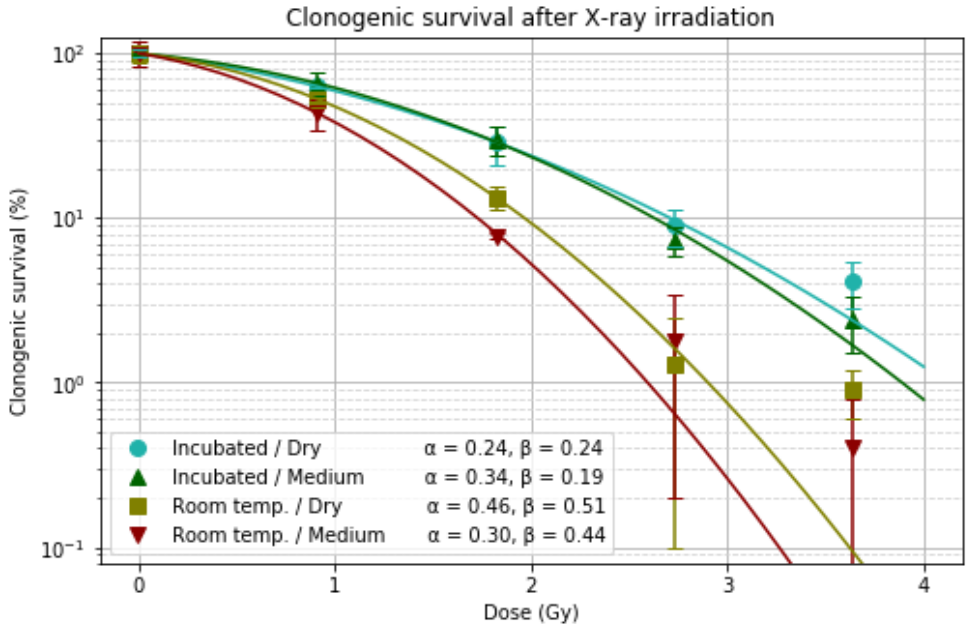

Figure 24: Clonogenic survival of U2OS cells after X-ray (195 kV) irradiation, every marker is the average surviving fraction of three wells. Half of the 6-well plates were stored outside the incubator (at room temperature) for four hours. For both situations, cells with medium and without medium (dry) were irradiated. Parameters α and β from the LQ-model are given for each linear-quadratic fit.

From Figure 24 it follows that incubated cells were able to form more colonies after irradiation compared to cells that had been on room temperature for four hours. Dry cells that had been incubated required a factor 1.38 more dose to reach 10% clonogenic survival, this factor is 1.48 for the colonies where there was medium in the wells during irradiation. Cells that were irradiated without medium (dry) in the well had a higher surviving fraction than cells that had medium in the well. The factor between dry and medium to reach 10% clonogenic survival is 1.04 for the incubated cells and 1.11 for the cells that had been on room temperature.

Values for α and β in Figure 24 do not correspond to values found by Cuaron *et al* [66] and Howard *et al* [95], that both used U2OS cells and 6-MV X-rays. Their values are α=0.1830 Gy^{-1}, β=0.0332 Gy^{-2} and α=0.632 Gy^{-1}, β=0.0.034 Gy^{-2} respectively, compared to the α=0.24 Gy^{-1} and β=0.19 Gy^{-2} found in this study, for the situation that is most similar to theirs (incubated / medium).

5 Discussion

The polystyrene slabs of the sample-holder have a mean WET of 1.03 cm, the SEM is 0.002 cm. For the calculations in this thesis a WET of 1.03 cm is used for all 10 mm slabs, with perfect uniformity. The density of 5 mm and 10 mm thick slabs is 1.04 g/cm^3 and the density of 0.5 mm and 1 mm thick slabs is 1.06 g/cm^3.

Absolute dose measurement with EBT3 film in the polystyrene phantom is 11% higher than the delivered dose, where the measured dose in the RW3 phantom agrees with the delivered dose within 1%. Based on this experiment it appears that the delivered dose by the large homogeneous box plan to the polystyrene phantom is in the order of 10% higher compared to the delivered dose to the RW3 phantom. The most likely explanation for the elevated dose delivery in the polystyrene phantom is an error in the process of using EBT3 film. It is possible that that particular film had been wrongly oriented, as optical density measurements of EBT3 films is shown to be orientation dependent[96]. Since the elevated dose measurement in polystyrene is an unexpected result, it is recommended that the experiment is repeated with multiple films for multiple doses (at least 2 and 4 Gy).

Using the density that is calculated from the WET measurements it is possible to calculate the range of a 70 MeV Bragg peak within a 0.5 mm accuracy with both RayStation and TOPAS MC. The same experiment should be performed with higher energies, to verify that range calculation also works at greater depths.

The depth dose calculation of a 70 MeV pencil beam by RayStation in Figure 21 loses its smoothness in the distal fall-off. Since the binning size in depth is 0.1 mm and thus this is not the cause of the pointedness, it is assumed that this artifact is a result of the pencil beam algorithm.
Normalized TOPAS central axis dose calculations and EBT3 film dose measurements agree within 5%. The central axis dose calculated with RayStation does not agree with the measurement points using EBT3 films. After extra scaling of the dose shown in Figure 22, both the calculations of RayStation and TOPAS agree better with the measured doses with EBT3 film. The TOPAS calculation also agrees everywhere within 1% with the measured doses. The RayStation calculation agrees within 1% in the plateau region and proximal part of the Bragg peak, but differs 20% from the measured dose in the Bragg peak and over 100% in the distal fall-off. The results of the pencil beam algorithm of an older version of RayStation (v4.0) have been proven to be insufficient to calculate doses in heterogeneous media[97]. However, the target used for dose calculations in this study was homogeneous. Even though the TOPAS calculation agrees better with the measurement results, at this moment there is no foundation to prove that either the TOPAS or RayStation calculation is more correct. More calculations in both TOPAS and RayStation are needed as well as deepened knowledge on the dose calculation methods used in RayStation.

The LET_d value calculated for the position of cells in the plateau region of a 150 MeV field is 1.30 keV/μm. The LET_d value for the position of the cells in the Bragg peak of a 90 MeV Bragg peak is 3.78 keV/μm. Despite the fact that the modeled geometry and beam parameters in TOPAS MC were simplified and limited, these LET_d values seem reasonable when compared to the literature[98].

Although the results in Figure 23 are insignificant, the 0.45 Gy measurement points show that cells that had no medium inside the wells during irradiation were able to form more colonies than cells that did have medium inside the wells during irradiation. This result can also be seen for X-ray irradiation in Figure 24. A possible explanation for this is the fact that new medium is added after irradiation. The medium contains nutrients and regulators that cells need for proliferation, when adding new medium this generates a flow that replaces 'old' and consumed medium for new medium full of nutrients and regulators.

The α and β values found in this study do not correspond to values found in literature [66, 95]. The value for α found in this study is in between the two values found in literature, but the value found for β is considerably higher than those found in literature. This difference may come from the difference in X-ray energy that is used to irradiate the samples. In literature 6 MV X-rays ($\text{LET}_d = 0.2$ keV/μm [99]) are used where in this study 195 kV X-rays ($\text{LET}_d = 3.5$ keV/μm [100]) are used. The most obvious conclusion that can be drawn from Figure 24 is that cells that have been at room temperature for four hours suffered from considerably more cell death than cells that were kept incubated. Cell death for cells at room temperature was up to 5 times higher for doses of 1.82 Gy and higher compared to cells that had been incubated. With this information, the fact that cells were not incubated for a duration of five hours during the proton irradiation is a likely explanation for the low cell survival numbers shown in figure 23. Cells were transport by car from Rotterdam to Delft which can add up to the increased cell death because of temperature. Because the results of irradiation in the Bragg peak vs plateau region are so limited, the relation between RBE and LET_d for protons could not be studied. The advise is to perform future radiobiological experiments fully on-site when all equipment is available. Cells should be cultivated and seeded in-house and be incubated at all times (besides during irradiation).

Bibliography

[1] Robert R. Wilson. Radiological use of fast protons. *Radiology*, 47(5):487–491, 1946. doi: 10.1148/47.5.487. PMID: 20274616.

[2] Harald Paganetti. Range uncertainties in proton therapy and the role of monte carlo simulations. *Physics in Medicine and Biology*, 57(11):R99–R117, may 2012. doi: 10.1088/0031-9155/57/11/r99.

[3] K. Ilicic, S. E. Combs, and T. E. Schmid. New insights in the relative radiobiological effectiveness of proton irradiation. *Radiation Oncology*, 13(1):6, Jan 2018. ISSN 1748-717X. doi: 10.1186/s13014-018-0954-9.

[4] Henning Willers, Antonio Allen, David Grosshans, Stephen J. McMahon, Cläre von Neubeck, Claudia Wiese, and Bhadrasain Vikram. Toward a variable rbe for proton beam therapy. *Radiotherapy and Oncology*, 128(1):68 – 75, 2018. ISSN 0167-8140. doi: https://doi.org/10.1016/j.radonc.2018.05.019.

[5] HollandPTC. Research pillars: Hollandptc rd programme, 2018. `https://www.hollandptc.nl/wp-content/uploads/2018/07/Research-Pillars-HollandPTC-RD-programme.pdf`.

[6] C-M Ma, T Lomax, William R Hendee, and Richard Amos. Proton and carbon ion therapy. *Medical physics*, 40:057301, 05 2013. doi: 10.1118/1.4802213.

[7] Timur Mitin and Anthony L. Zietman. Promise and pitfalls of heavy-particle therapy. *Journal of Clinical Oncology*, 32(26):2855–2863, 2014. doi: 10.1200/JCO.2014.55.1945. PMID: 25113772.

[8] H. Bethe. Zur theorie des durchgangs schneller korpuskularstrahlen durch materie. *Annalen der Physik*, 397(3):325–400, 1930. doi: 10.1002/andp.19303970303.

[9] F. Bloch. Zur bremsung rasch bewegter teilchen beim durchgang durch materie. *Annalen der Physik*, 408(3):285–320, 1933. doi: 10.1002/andp.19334080303.

[10] F. Bloch. Bremsvermögen von atomen mit mehreren elektronen. *Physik*, 1933. doi: https://doi.org/10.1007/BF01344553.

[11] W.H. Barkas. *Nuclear Research Emulsions*. Number v. 1-2 in Nuclear Research Emulsions. Academic Press, 1963.

[12] Aafke Christine Kraan. Range verification methods in particle therapy: Underlying physics and monte carlo modeling. 5:150, 07 2015.

[13] Nist database. Available from: `https://radiopaedia.org`.

[14] A. Allisy, W. A. Jennings, A. M. Kellerer, J. W. Müller, H. H. Rossi, and S. M. Seltzer. Report 60. *Journal of the International Commission on Radiation Units and Measurements*, os31(1):NP, 1998. doi: 10.1093/jicru/os31.1.Report60.

[15] Malte Christian Frese, Jan J. Wilkens, Peter E Huber, Alexandra D. Jensen, Uwe Oelfke, and Zahra Taheri-Kadkhoda. Application of constant vs. variable relative biological effectiveness in treatment planning of intensity-modulated proton therapy. *International journal of radiation oncology, biology, physics*, 79 1:80–8, 2011.

[16] Sp-0041: Physical advantages of particles: protons vs. heavy ions, what is certain what is not? *Radiotherapy and Oncology*, 119:S17, 2016. ISSN 0167-8140. doi: https://doi.org/10.1016/S0167-8140(16)31290-7. ESTRO 35, 29 April - 3 May 2016, Turin, Italy.

[17] C Grassberger and H Paganetti. Elevated let components in clinical proton beams. *Physics in Medicine Biology*, 56(20):6677, 2011.

[18] Jan J. Wilkens and Uwe Oelfke. Analytical linear energy transfer calculations for proton therapy. *Medical Physics*, 30(5):806–815. doi: 10.1118/1.1567852.

[19] Marco Tommasino, Francesco anFd Durante. Proton radiobiology. *Cancers*, 7 (1):353—381, 2015. ISSN 2072-6694. doi: 10.3390/cancers7010353.

[20] Wei Han and Kwan Ngok Yu. *Response of cells to ionizing radiation*, pages 204–262. Bentham Science Publishers Ltd., 2009. doi: 10.2174/978160805040610901010204.

[21] Evidence for dna double-strand breaks as the critical lesions in yeast cells irradiated with sparsely or densely ionizing radiation under oxic or anoxic conditions. *Radiation Research*, 88(3):524–532, 1981. ISSN 00337587, 19385404.

[22] P.E. Bryant. Enzymatic restriction of mammalian cell dna: Evidence for double-strand breaks as potentially lethal lesions. *International Journal of Radiation Biology and Related Studies in Physics, Chemistry and Medicine*, 48(1):55–60, 1985. doi: 10.1080/09553008514551061.

[23] A. Campa, F. Ballarini, M. Belli, R. Cherubini, V. Dini, G. Esposito, W. Friedland, S. Gerardi, S. Molinelli, A. Ottolenghi, H. Paretzke, G. Simone, and M. A. Tabocchini. Dna dsb induced in human cells by charged particles and gamma rays: Experimental results and theoretical approaches. *International Journal of Radiation Biology*, 81(11):841–854, 2005. doi: 10.1080/09553000500530888.

[24] Mauro Belli, F Ianzini, O Sapora, Maria Antonella Tabocchini, F Cera, Roberto Cherubini, Al Mamun I Haque, G Moschini, P Tiveron, and Giustina Simone. Dna double strand break production and rejoining in v79 cells irradiated with light ions. *Advances in space research : the official journal of the Committee on Space Research (COSPAR)*, 18:73–82, 12 1996. doi: 10.1016/0273-1177(95)00793-E.

[25] Elzbieta Pastwa, Ronald D. Neumann, Katherina Mezhevaya, and Thomas A. Winters. Repair of radiation-induced dna double-strand breaks is dependent upon radiation quality and the structural complexity of double-strand breaks. *Radiation Research*, 159(2):251–261, 2003. doi: 10.1667/0033-7587(2003)159[0251:RORIDD]2.0.CO;2.

[26] Bjorn Rydberg. Radiation-induced dna damage and chromatin structure. *Acta oncologica*, 40 6:682–5, 2001.

[27] Jacek Capala Jeff Buchsbaum, Eric J. Bernhard. Defining high-let radiation molecular and cellular damage and responses relevant to oncology. `https://deainfo.nci.nih.gov/advisory/joint/1218/Buchsbaum.pdf`.

[28] John F. Fowler. The linear-quadratic formula and progress in fractionated radiotherapy. 62:679–94, 09 1989.

[29] G. Kraft. Tumor therapy with heavy charged particles. *Progress in Particle and Nuclear Physics*, 45:S473 – S544, 2000. ISSN 0146-6410. doi: https://doi.org/10.1016/S0146-6410(00)00112-5.

[30] Minna Wedenberg, Bengt K. Lind, and Björn Hårdemark. A model for the relative biological effectiveness of protons: The tissue specific parameter / of photons is a predictor for the sensitivity to let changes. *Acta Oncologica*, 52(3): 580–588, 2013. doi: 10.3109/0284186X.2012.705892. PMID: 22909391.

[31] Harald Paganetti. Relative biological effectiveness (rbe) values for proton beam therapy. variations as a function of biological endpoint, dose, and linear energy transfer. *Physics in Medicine Biology*, 59(22):R419, 2014.

[32] M Belli, R Cherubini, S Finotto, G Moschini, O Sapora, G Simone, and MA Tabocchini. Rbe-let relationship for the survival of v79 cells irradiated with low energy protons. *International journal of radiation biology*, 55(1):93–104, 1989.

[33] Harald Paganetti, Eleanor Blakely, Alejandro Carabe-Fernandez, David J. Carlson, Indra J. Das, Lei Dong, David Grosshans, Kathryn D. Held, Radhe Mohan, Vitali Moiseenko, Andrzej Niemierko, Robert D. Stewart, and Henning Willers. Report of the aapm tg-256 on the relative biological effectiveness of proton beams in radiation therapy. *Medical Physics*, 0(0). doi: 10.1002/mp.13390.

[34] Michael Goitein. Radiation oncology: A physicist's-eye view. 2007. doi: https://doi.org/10.1007/978-0-387-72645-8.

[35] Dirk P. Kroese, Tim Brereton, Thomas Taimre, and Zdravko I. Botev. Why the monte carlo method is so important today. *Wiley Interdisciplinary Reviews: Computational Statistics*, 6(6):386–392, 2014. doi: 10.1002/wics.1314.

[36] J. Perl, J. Shin, J. Schümann, B. Faddegon, and H. Paganetti. Topas: An innovative proton monte carlo platform for research and clinical applications. *Medical Physics*, 39(11):6818–6837, 2012. doi: 10.1118/1.4758060.

[37] Harald Paganetti, K. Parodi, H. Jiang, J. A. Adams, and H. M. Kooy. Comparison of pencil-beam and monte carlo calculated dose distributions for proton therapy of skull-base and para-spinal tumors. In R. Magjarevic and J. H. Nagel, editors, *World Congress on Medical Physics and Biomedical Engineering 2006*, pages 2219–2222, Berlin, Heidelberg, 2007. Springer Berlin Heidelberg.

[38] S. Agostinelli et al. Geant4—a simulation toolkit. *Nuclear Instruments and Methods in Physics Research Section A: Accelerators, Spectrometers, Detectors and Associated Equipment*, 506(3):250 – 303, 2003. ISSN 0168-9002. doi: https://doi.org/10.1016/S0168-9002(03)01368-8.

[39] Simona Giordanengo and Hugo Palmans. Dose detectors, sensors, and their applications. *Medical Physics*, 45(11):e1051–e1072, 2018. doi: 10.1002/mp.13089.

[40] T. Bortfeld. An analytical approximation of the bragg curve for therapeutic proton beams. *Medical Physics*, 24(12):2024–2033, 1997.

[41] IBA. Giraffe: Single-shot bragg peak measurement, 2019. `https://www.iba-dosimetry.com/product/giraffe/`.

[42] Rui Zhang and Wayne D Newhauser. Calculation of water equivalent thickness of materials of arbitrary density, elemental composition and thickness in proton beam irradiation. *Physics in Medicine and Biology*, 54(6):1383–1395, feb 2009. doi: 10.1088/0031-9155/54/6/001.

[43] INTERNATIONAL ATOMIC ENERGY AGENCY. *Calibration of Radiation Protection Monitoring Instruments*. Number 16 in Safety Reports Series. INTERNATIONAL ATOMIC ENERGY AGENCY, Vienna, 2000.

[44] INTERNATIONAL ATOMIC ENERGY AGENCY. *Implementation of the International Code of Practice on Dosimetry in Radiotherapy (TRS 398): Review of Test Results*. INTERNATIONAL ATOMIC ENERGY AGENCY, Vienna, 2005. IAEA-TECDOC-1455.

[45] S. Giordanengo, L. Manganaro, and A. Vignati. Review of technologies and procedures of clinical dosimetry for scanned ion beam radiotherapy. *Physica Medica*, 43:79 – 99, 2017. ISSN 1120-1797. doi: https://doi.org/10.1016/j.ejmp.2017.10.013.

[46] Slobodan Devic. Radiochromic film dosimetry: Past, present, and future. *Physica Medica*, 27(3):122 – 134, 2011. ISSN 1120-1797. doi: https://doi.org/10.1016/j.ejmp.2010.10.001.

[47] Ashland. Ebt3 specification and user guide. `http://www.gafchromic.com/documents/EBT3_Specifications.pdf`.

[48] D.P. Jones. *Biomedical Sensors*. Sensor technology series. Momentum Press, 2010. ISBN 9781606500569.

[49] Hiromitsu Iwata, Hiroyuki Ogino, Shingo Hashimoto, Maho Yamada, Hiroki Shibata, Keisuke Yasui, Toshiyuki Toshito, Chihiro Omachi, Kotoha Tatekawa, Yoshihiko Manabe, Jun etsu Mizoe, and Yuta Shibamoto. Spot scanning and passive scattering proton therapy: Relative biological effectiveness and oxygen enhancement ratio in cultured cells. *International Journal of Radiation Oncology*Biology*Physics*, 95(1):95 – 102, 2016. ISSN 0360-3016. doi: https://doi.org/10.1016/j.ijrobp.2016.01.017. Particle Therapy Special Edition.

[50] Anna Michaelidesová, Jana Vachelova, Monika Puchalska, Katerina Pachnerova Brabcova, Vladimir Vondracek, Lembit Sihver, and Marie Davidkova. Relative biological effectiveness in a proton spread-out bragg peak formed by pencil beam scanning mode. *Australasian Physical Engineering Sciences in Medicine*, 40, 03 2017. doi: 10.1007/s13246-017-0540-8.

[51] L. Verhey, H. Blattman, P. M. Deluca, and D. Miller. Report 59. *Journal of the International Commission on Radiation Units and Measurements*, os30(2): NP, 1998. doi: 10.1093/jicru/os30.2.Report59.

[52] Kenkyu Sha Tsusho Sangyo. Jsmp standard dosimetry of absorbed dose in external beam radiotherapy (standard dosimetry 01). 2002.

[53] Ivan Petrović, Aleksandra Ristić-Fira, Danijela Todorović, Lela Korićanac, Lucia Valastro, Pablo Cirrone, and Giacomo Cuttone. Response of a radioresistant human melanoma cell line along the proton spread-out bragg peak. *International Journal of Radiation Biology*, 86(9):742–751, 2010. doi: 10.3109/09553002.2010.481322. PMID: 20597839.

[54] Ariungerel Gerelchuluun, Zhengshan Hong, Lue Sun, Kenshi Suzuki, Toshiyuki Terunuma, Kiyoshi Yasuoka, Takeji Sakae, Takashi Moritake, and Koji Tsuboi. Induction of in situ dna double-strand breaks and apoptosis by 200 mev protons and 10 mv x-rays in human tumour cell lines. *International Journal of Radiation Biology*, 87(1):57–70, 2011. doi: 10.3109/09553002.2010.518201.

[55] Valentin Calugaru, Catherine Nauraye, Georges Noël, Nicole Giocanti, Vincent Favaudon, and Frédérique Mégnin-Chanet. Radiobiological characterization of two therapeutic proton beams with different initial energy spectra used at the institut curie proton therapy center in orsay. *International Journal of Radiation Oncology*Biology*Physics*, 81(4):1136 – 1143, 2011. ISSN 0360-3016. doi: https://doi.org/10.1016/j.ijrobp.2010.09.003.

[56] Karl T Butterworth, Conor K McGarry, Ben Clasie, Alejandro Carabe-Fernandez, Jan Schuemann, Nicolas Depauw, Shikui Tang, Stephen J McMahon, Giuseppe Schettino, Joe M O'Sullivan, Hsaio-Ming Lu, Hanne Kooy, Harald Paganetti, Alan R Hounsell, Kathryn D Held, and Kevin M Prise. Relative biological effectiveness (rbe) and out-of-field cell survival responses to passive scattering and pencil beam scanning proton beam deliveries. *Physics in Medicine Biology*, 57(20):6671, 2012.

[57] Richard. A. Britten, Vahagn Nazaryan, Leslie K. Davis, Susan B. Klein, Dmitri Nichiporov, Marc S. Mendonca, Mark Wolanski, Xiliang Nie, Jerry George, and Cynthia Keppel. Variations in the rbe for cell killing along the depth-dose profile of a modulated proton therapy beam. *Radiation Research*, 179(1):21–28, 2013. doi: 10.1667/RR2737.1. PMID: 23148508.

[58] Svetlana Sorokina, Eva Markova, Jan Gursky, Jozef Dobrovodsky, and Igor Belyaev. Relative biological efficiency of protons at low and therapeutic doses in induction of 53bp1/h2ax foci in lymphocytes from umbilical cord blood. *International Journal of Radiation Biology*, 89(9):716–723, 2013. doi: 10.3109/09553002.2013.797619.

[59] Dorota Słonina, Beata Biesaga, Jan Swakoń, D Kabat, Leszek Grzanka, Marta Ptaszkiewicz, and Urszula Sowa. Relative biological effectiveness of the 60-mev therapeutic proton beam at the institute of nuclear physics (ifj pan) in krak??w, poland. *Radiation and environmental biophysics*, 53, 07 2014. doi: 10.1007/s00411-014-0559-0.

[60] Yoshitaka Matsumoto, Taeko Matsuura, Mami Wada, Yusuke Egashira, Teiji Nishio, and Yoshiya Furusawa. Enhanced radiobiological effects at the distal end of a clinical proton beam: in vitro study. *Journal of Radiation Research*, 55(4):816–822, 2014. doi: 10.1093/jrr/rrt230.

[61] Otilija Keta, Danijela Todorovic, Nataša Popović, Lela Korićanac, Giacomo Cuttone, Ivan Petrović, and Aleksandra Ristic-Fira. Radiosensitivity of human ovarian carcinoma and melanoma cells to -rays and protons. *Archives of medical science : AMS*, 10:578–86, 06 2014. doi: 10.5114/aoms.2014.43751.

[62] Mizuho Aoki-Nakano, Yoshiya Furusawa, Akiko Uzawa, Yoshitaka Matsumoto, Ryoichi Hirayama, Chizuru Tsuruoka, Takashi Ogino, Teiji Nishio, Kazufumi Kagawa, Masao Murakami, Go Kagiya, Kyo Kume, Masanori Hatashita, Shigekazu Fukuda, Kazutaka Yamamoto, Hiroshi Fuji, Shigeyuki Murayama, Masaharu Hata, Takeji Sakae, and Hideki Matsumoto. Relative biological effectiveness of therapeutic proton beams for hsg cells at japanese proton therapy facilities. *Journal of Radiation Research*, 55(4):812–815, 2014. doi: 10.1093/jrr/rru003.

[63] Pankaj Chaudhary, Thomas I. Marshall, Francesca M. Perozziello, Lorenzo Manti, Frederick J. Currell, Fiona Hanton, Stephen J. McMahon, Joy N. Kavanagh, Giuseppe Antonio Pablo Cirrone, Francesco Romano, Kevin M. Prise, and Giuseppe Schettino. Relative biological effectiveness variation along monoenergetic and modulated bragg peaks of a 62-mev therapeutic proton beam: A preclinical assessment. *International Journal of Radiation Oncology*Biology*Physics*, 90(1):27 – 35, 2014. ISSN 0360-3016. doi: https://doi.org/10.1016/j.ijrobp.2014.05.010.

[64] Bradly G. Wouters, Lloyd D Skarsgard, Leo E. Gerweck, Alejandro Cárabe-Fernández, Michelle X Wong, Ralph E. Durand, Deanna Nielson, Marc R. Bussiere, Miles S Wagner, Peter J. Biggs, Harald Paganetti, and Herman D. Suit. Radiobiological intercomparison of the 160 mev and 230 mev proton therapy beams at the harvard cyclotron laboratory and at massachusetts general hospital. *Radiation research*, 183 2:174–87, 2015.

[65] Variations in the processing of dna double-strand breaks along 60-mev therapeutic proton beams. *International Journal of Radiation Oncology*Biology*Physics*, 95(1):86 – 94, 2016. ISSN 0360-3016. doi: https://doi.org/10.1016/j.ijrobp.2015.07.2279. Particle Therapy Special Edition.

[66] John J. Cuaron, Chang Chang, Michael Lovelock, Daniel S. Higginson, Dennis Mah, Oren Cahlon, and Simon Powell. Exponential increase in relative biological effectiveness along distal edge of a proton bragg peak as measured by deoxyribonucleic acid double-strand breaks. *International Journal of Radiation Oncology*Biology*Physics*, 95(1):62 – 69, 2016. ISSN 0360-3016. doi: https://doi.org/10.1016/j.ijrobp.2016.02.018. Particle Therapy Special Edition.

[67] Steffen Nielsen, Niels Bassler, Leszek Grzanka, Louise Laursen, Jan Swakon, Pawel Olko, Christian Nicolaj Andreassen, Jan Alsner, and Brita Sørensen. Comparison of coding transcriptomes in fibroblasts irradiated with low and high let proton beams and cobalt-60 photons. *International Journal of Radiation Oncology*Biology*Physics*, 2018. ISSN 0360-3016. doi: https://doi.org/10.1016/j.ijrobp.2018.11.065.

[68] Agnieszka Panek, Justyna Miszczyk, and Jan Swakoń. Biological effects and inter-individual variability in peripheral blood lymphocytes of healthy donors exposed to 60-mev proton radiotherapeutic beam. *International Journal of Radiation Biology*, 94(12):1085–1094, 2018. doi: 10.1080/09553002.2019.1524941.

[69] A. Rykkelid, S. Siem, K. Ytre-Hauge, E. Malinen, and N. Edin. Ep-2280: Very high relative biological effectiveness found at the distal end of the proton bragg peak. *Radiotherapy and Oncology*, 127:S1259, 2018. ISSN 0167-8140. doi: https://doi.org/10.1016/S0167-8140(18)32589-1. ESTRO 37, April 20-24, 2018, Barcelona, Spain.

[70] Armin Lühr, Cläre von Neubeck, Mechthild Krause, and Esther G.C. Troost. Relative biological effectiveness in proton beam therapy – current knowledge and future challenges. *Clinical and Translational Radiation Oncology*, 9:35 – 41, 2018. ISSN 2405-6308. doi: https://doi.org/10.1016/j.ctro.2018.01.006.

[71] Marco Durante, Harald Paganetti, Arnold Pompos, Stephen F. Kry, Xiaodong Wu, and David R. Grosshans. Report of a national cancer institute special panel: Characterization of the physical parameters of particle beams for biological research. *Medical Physics*, 0(0). doi: 10.1002/mp.13324.

[72] Zvi Fuks and Richard Kolesnick. Engaging the vascular component of the tumor response. *Cancer Cell*, 8(2):89 – 91, 2005. ISSN 1535-6108. doi: https://doi.org/10.1016/j.ccr.2005.07.014.

[73] Heon Joo Park, Robert J. Griffin, Susanta Hui, Seymour H. Levitt, and Chang W. Song. Radiation-induced vascular damage in tumors: Implications of vascular damage in ablative hypofractionated radiotherapy (sbrt and srs). *Radiation Research*, 177(3):311–327, 2012. doi: 10.1667/RR2773.1. PMID: 22229487.

[74] M. Zahidunnabi Dewan, Ashley E. Galloway, Noriko Kawashima, J. Keith Dewyngaert, James S. Babb, Silvia C. Formenti, and Sandra Demaria. Fractionated but not single-dose radiotherapy induces an immune-mediated abscopal effect when combined with anti–ctla-4 antibody. *Clinical Cancer Research*, 15 (17):5379–5388, 2009. ISSN 1078-0432. doi: 10.1158/1078-0432.CCR-09-0265.

[75] Susan M. Hiniker, Daniel Shin yu Chen, Sunil Reddy, Daniel Tandel Chang, Jennifer C Jones, Joseph A. Mollick, Susan M. Swetter, and Susan J. Knox. A systemic complete response of metastatic melanoma to local radiation and immunotherapy. *Translational oncology*, 5 6:404–7, 2012.

[76] Michael A Postow, James Harding, and Jedd D Wolchok. Targeting immune checkpoints: releasing the restraints on anti-tumor immunity for patients with melanoma. *Cancer journal (Sudbury, Mass.)*, 18(2):153—159, 2012. ISSN 1528-9117. doi: 10.1097/ppo.0b013e31824b2404.

[77] Niklas Finnberg, Chris Wambi, Jeffrey H Ware, Ann Kennedy, and Wafik S El-Deiry. Gamma-radiation (gr) triggers a unique gene expression profile associated with cell death compared to proton radiation (pr) in mice in vivo. *Cancer biology therapy*, 7:2023–33, 01 2009. doi: 10.4161/cbt.7.12.7417.

[78] Nicole Grosse, Andrea O. Fontana, Eugen B. Hug, Antony Lomax, Adolf Coray, Marc Augsburger, Harald Paganetti, Alessandro A. Sartori, and Martin Pruschy. Deficiency in homologous recombination renders mammalian cells more sensitive to proton versus photon irradiation. *International Journal of Radiation Oncology*Biology*Physics*, 88(1):175 – 181, 2014. ISSN 0360-3016. doi: https://doi.org/10.1016/j.ijrobp.2013.09.041.

[79] Rebecca Grün, Thomas Friedrich, Erik Traneus, and Michael Scholz. Is the dose-averaged let a reliable predictor for the relative biological effectiveness? *Medical Physics*, 0(0). doi: 10.1002/mp.13347.

[80] Thomas Friedrich, Uwe Scholz, Thilo ElsäSser, Marco Durante, and Michael Scholz. Systematic analysis of rbe and related quantities using a database of cell survival experiments with ion beam irradiation. *Journal of Radiation Research*, 54(3):494–514, 2013. doi: 10.1093/jrr/rrs114.

[81] Antony Lomax. What will the medical physics of proton therapy look like 10yr from now? a personal view. *Medical Physics*, 45(11):e984–e993, 2018. doi: 10.1002/mp.13206.

[82] Swati Girdhani, Clare Lamont, Philip Hahnfeldt, Amir Abdollahi, and Lynn Hlatky. Proton irradiation suppresses angiogenic genes and impairs cell invasion and tumor growth. *Radiation research*, 178:33–45, 06 2012. doi: 10.2307/23261975.

[83] Lianghao Ding, Seongmi Park, Michael Peyton, Luc Girard, Yang Xie, John Minna, and Michael Story. Distinct transcriptome profiles identified in normal human bronchial epithelial cells after exposure to -rays and different elemental particles of high z and energy. *BMC genomics*, 14:372, 06 2013. doi: 10.1186/1471-2164-14-372.

[84] Wilfried Goetz, Michelle N M Morgan, and Janet Baulch. The effect of radiation quality on genomic dna methylation profiles in irradiated human cell lines. *Radiation research*, 175:575–87, 03 2011. doi: 10.1667/RR2390.1.

[85] Erich Giedzinski, Radoslaw Rola, John R. Fike, and Charles L. Limoli. Efficient production of reactive oxygen species in neural precursor cells after exposure to 250 mev protons. *Radiation Research*, 164(4):540–544, 2005. ISSN 00337587, 19385404.

[86] Andrea O. Fontana, Marc A. Augsburger, Nicole Grosse, Matthias Guckenberger, Anthony J. Lomax, Alessandro A. Sartori, and Martin N. Pruschy. Differential dna repair pathway choice in cancer cells after proton- and photon-irradiation. *Radiotherapy and Oncology*, 116(3):374 – 380, 2015. ISSN 0167-8140. doi: https://doi.org/10.1016/j.radonc.2015.08.014. Papers from the 14th International Wolfsberg Meeting on Molecular Radiation Biology/Oncology, June 20-22, 2015.

[87] Qi Liu, Priyanjali Ghosh, Nicole Magpayo, Mauro Testa, Shikui Tang, Liliana Gheorghiu, Peter Biggs, Harald Paganetti, Jason A. Efstathiou, Hsiao-Ming Lu, Kathryn D. Held, and Henning Willers. Lung cancer cell line screen links fanconi anemia/brca pathway defects to increased relative biological effectiveness of proton radiation. *International Journal of Radiation Oncology*Biology*Physics*, 91(5):1081 – 1089, 2015. ISSN 0360-3016. doi: https://doi.org/10.1016/j.ijrobp.2014.12.046.

[88] Carol-Anne Martin Daniel Wenzel Louise S. Bicknell Matthew E. Hurles Tessa Homfray Josef M. Penninger Andrew P. Jackson Juergen A. Knoblich Madeline A. Lancaster, Magdalena Renner. Cerebral organoids model human brain development and microcephaly. *Nature*, 2013. doi: 10.1038/nature12517.

[89] Thermo Fischer. Culture media sera. https://www.thermofisher.com/nl/en/home/references/gibco-cell-culture-basics/cell-culture-environment/culture-media.html.

[90] lap laser. Easy cube: containing technical data on rw3, 2018. https://www.lap-laser.com/products/easy-cube.

[91] INTERNATIONAL ATOMIC ENERGY AGENCY. *Absorbed Dose Determination in External Beam Radiotherapy*. Number 398 in Technical Reports Series. INTERNATIONAL ATOMIC ENERGY AGENCY, Vienna, 2000.

[92] M A Cortés-Giraldo and A Carabe. A critical study of different monte carlo scoring methods of dose average linear-energy-transfer maps calculated in voxelized geometries irradiated with clinical proton beams. *Physics in Medicine Biology*, 60(7):2645, 2015.

[93] Dal A Granville and Gabriel O Sawakuchi. Comparison of linear energy transfer scoring techniques in monte carlo simulations of proton beams. *Physics in Medicine Biology*, 60(14):N283, 2015.

[94] NIST. Composition of polystyrene, 2018. https://physics.nist.gov/cgi-bin/Star/compos.pl?matno=226.

[95] Michelle Howard, Chris Beltran, Jann Sarkaria, and Michael G Herman. Characterization of relative biological effectiveness for conventional radiation therapy: a comparison of clinical 6 MV X-rays and 137Cs. *Journal of Radiation Research*, 58(5):608–613, 04 2017. ISSN 0449-3060. doi: 10.1093/jrr/rrx018.

[96] Valeria Casanova Borca, Massimo Pasquino, Giuliana Russo, Pierangelo Grosso, Domenico Cante, Piera Sciacero, Giuseppe Girelli, Maria Rosa La Porta, and Santi Tofani. Dosimetric characterization and use of gafchromic ebt3 film for imrt dose verification. *Journal of Applied Clinical Medical Physics*, 14(2):158–171, 2013. doi: 10.1120/jacmp.v14i2.4111.

[97] Jay Saini, A.J. Egan, Dominic Maes, Stephen Bowen, Tony Wong, and Charles Bloch. Dose calculation accuracy of commercial monte-carlo and pencil beam algorithms in bone and lung phantoms: Comparisons against geant4 simulations and measurements. *International Journal of Radiation Oncology*Biology*Physics*, 99:E718, 10 2017. doi: 10.1016/j.ijrobp.2017.06.2331.

[98] Fada Guan, Christopher Peeler, Lawrence Bronk, Changran Geng, Reza Taleei, Sharmalee Randeniya, Shuaiping Ge, Dragan Mirkovic, David Grosshans, Radhe Mohan, and Uwe Titt. Analysis of the track- and dose-averaged let and let spectra in proton therapy using the geant4 monte carlo code. *Medical Physics*, 42(11):6234–6247. doi: 10.1118/1.4932217.

[99] Xiao-dong Jin, Li Gong, Chuan-ling Guo, Ji-fang Hao, Wei Wei, Zhong-ying Dai, and Qiang Li. Survivin expressions in human hepatoma hepg2 cells exposed to ionizing radiation of different let. *Radiation and Environmental Biophysics*, 47(3):399–404, Jul 2008. ISSN 1432-2099. doi: 10.1007/s00411-008-0165-0.

[100] J. Valentin. Relative biological effectiveness (rbe), quality factor (q), and radiation weighting factor (wr): Icrp publication 92. *Annals of the ICRP*, 33(4):1 – 121, 2003. ISSN 0146-6453.

Appendices

Appendix A: List of abbreviations

Abbreviation	Meaning
(D)DSB	(DNA) Double Strand Break
EPR	Electron Paramagnetic Resonance
LET	Linear Energy Transfer
LET_D	Dose-averaged Linear Energy Transfer
Linac	Linear accelarator
LQ	Linear-Quadratic
PBS	Pencil Beam Scanning
PS	Passive Scattering
RBE	Relative Biological Effectiveness
(SO)BP	(Spread-Out) Bragg Peak